



Article

Multi-Modal Analysis of Satellite Cells Reveals Early Impairments at Pre-Contractile Stages of Myogenesis in Duchenne Muscular Dystrophy

Sophie Franzmeier ^{1,2}, Shounak Chakraborty ³, Armina Mortazavi ^{4,5}, Jan B. Stöckl ⁶, Jianfei Jiang ^{4,5}, Nicole Pfarr ³, Benedikt Sabass ^{4,5}, Thomas Fröhlich ⁶, Clara Kaufhold ^{1,7}, Michael Stirm ^{8,9}, Eckhard Wolf ^{8,9}, Jürgen Schlegel ^{2,10}, ⁸ and Kaspar Matiasek ^{1,*}

- Section of Clinical & Comparative Neuropathology, Institute of Veterinary Pathology, Center for Clinical Veterinary Medicine, Ludwig-Maximilians-Universität München, 80539 Munich, Germany; sophie.franzmeier@lmu.de (S.F.); clara.kaufhold@gmail.com (C.K.)
- Department of Neuropathology, Institute of Pathology, School of Medicine and Health, Technical University Munich, 81675 Munich, Germany
- Institute of Pathology, School of Medicine and Health, Technical University Munich, 81675 Munich, Germany; shounak.chakraborty1990@gmail.com (S.C.); nicole.pfarr@tum.de (N.P.)
- Department of Veterinary Sciences, Institute for Infectious Diseases and Zoonoses, Ludwig-Maximilians-Universität München, 80752 Munich, Germany; armina.mortazavi@para.vetmed.uni-muenchen.de (A.M.); jiang.jianfei@lmu.de (J.J.); benedikt.sabass@micro.vetmed.uni-muenchen.de (B.S.)
- Faculty of Physics and Center for NanoScience, Ludwig-Maximilians-Universität München, 80752 Munich, Germany
- Laboratory of Functional Genome Analysis (LAFUGA), Gene Center, Ludwig-Maximilians-Universität München, 81377 Munich, Germany; stoeckl@genzentrum.lmu.de (J.B.S.); frohlich@genzentrum.lmu.de (T.F.)
- Metabolic Biochemistry, Faculty of Medicine, Biomedical Center (BMC), Ludwig-Maximilians-Universität München, 81377 Munich, Germany
- Molecular Animal Breeding and Biotechnology, Gene Center and Department of Veterinary Science, Ludwig-Maximilians-Universität München, 81377 Munich, Germany; michael_stirm@gmx.de (M.S.); ewolf@genzentrum.lmu.de (E.W.)
- Genter for Innovative Medical Models (CiMM), Department of Veterinary Sciences, Ludwig-Maximilians-Universität München, 85764 Oberschleißheim, Germany
- Exercise Biology, Department of Sport and Health Sciences, TUM School of Medicine and Health, Technical University Munich, 80809 Munich, Germany
- * Correspondence: schlegel@tum.de (J.S.); kaspar.matiasek@neuropathologie.de (K.M.); Tel.: +49-(0)89/2180-3313 (K.M.)

Abstract: Recent studies on myogenic satellite cells (SCs) in Duchenne muscular dystrophy (DMD) documented altered division capacities and impaired regeneration potential of SCs in DMD patients and animal models. It remains unknown, however, if SC-intrinsic effects trigger these deficiencies at pre-contractile stages of myogenesis rather than resulting from the pathologic environment. In this study, we isolated SCs from a porcine DMD model and age-matched wild-type (WT) piglets for comprehensive analysis. Using immunofluorescence, differentiation assays, traction force microscopy (TFM), RNA-seq, and label-free proteomic measurements, SCs behavior was characterized, and molecular changes were investigated. TFM revealed significantly higher average traction forces in DMD than WT SCs (90.4 \pm 10.5 Pa vs. 66.9 \pm 8.9 Pa; p = 0.0018). We identified 1390 differentially expressed genes and 1261 proteins with altered abundance in DMD vs. WT SCs. Dysregulated pathways uncovered by gene ontology (GO) enrichment analysis included sarcomere organization, focal adhesion, and response to hypoxia. Multi-omics factor analysis (MOFA) integrating transcriptomic and proteomic data, identified five factors accounting for the observed variance with an overall higher contribution of the transcriptomic data. Our findings suggest that SC impairments result from their inherent genetic abnormality rather



Academic Editor: Vincenzo Sorrentino

Received: 17 April 2025 Revised: 4 June 2025 Accepted: 9 June 2025 Published: 13 June 2025

Citation: Franzmeier, S.; Chakraborty, S.; Mortazavi, A.; Stöckl, J.B.; Jiang, J.; Pfarr, N.; Sabass, B.; Fröhlich, T.; Kaufhold, C.; Stirm, M.; et al. Multi-Modal Analysis of Satellite Cells Reveals Early Impairments at Pre-Contractile Stages of Myogenesis in Duchenne Muscular Dystrophy. Cells 2025, 14, 892. https://doi.org/ 10.3390/cells14120892

Copyright: © 2025 by the authors. Licensee MDPI, Basel, Switzerland. This article is an open access article distributed under the terms and conditions of the Creative Commons Attribution (CC BY) license (https://creativecommons.org/licenses/by/4.0/).

Cells 2025, 14, 892 2 of 28

than from environmental influences. The observed biological changes are intrinsic and not reactive to the pathological surrounding of DMD muscle.

Keywords: DMD; dystrophin; muscle stem cells; porcine model; muscle pathology; transcriptomics; proteomics; force generation

1. Introduction

Over the last two decades, studies on Duchenne muscular dystrophy (DMD) focused on the pathology of differentiated, dystrophic muscle fibers while leaving a gap in the comprehension of early disease mechanisms in pre-contractile stages of myogenesis. It was not until the discovery of high expression levels of dystrophin in activated satellite cells (SCs) [1], the stem cells of skeletal muscle tissue [2], that the interest in the role of SCs in the development of DMD grew considerably. In healthy tissue, dystrophin expression is detected at the mRNA and protein level in proliferating SC, nascent transcripts are generated in the myoblast prior to fusion, preparing for differentiation, and robust expression is found in mature myotubes and myofibers where it exhibits structural and regulatory functions [3–5]. On evolving concepts, several studies detected elevated numbers of myogenic SCs in muscle fibers of DMD patients [6,7] and *mdx* mice [8,9], which was explained by the hypothesis of SC exhaustion [10,11]. Recent investigations related these observations to the impairment of asymmetric divisions leading to an imbalance in maintaining the SC pool through self-renewal and the generation of muscle progenitor cells [1,12].

Still, it needs to be clarified if these impairments result from the pathological environment SCs reside in, or whether there are intrinsic SC defects, emerging at the undifferentiated muscle progenitor cell state. An investigation of dystrophin-deficient SCs and their function on disease onset and progression should lead to a better understanding of DMD pathobiology. As stem cell-based approaches may offer promising therapy options [13], the elucidation of affected biological pathways in DMD SCs is an urgent research topic.

First described in 1961 by Alexander Mauro [14], SCs are indispensable for muscle growth, regeneration, and repair. Located between the basal lamina and the sarcolemma, they reside in a quiescent state and are only activated upon muscle trauma or injury. Once stimulated, SCs proliferate extensively and, by undergoing asymmetric division, they give rise to myogenic precursor cells, which enter the myogenic pathway to differentiate into myofibers while simultaneously maintaining the stem cell pool through self-renewal [2,15]. The steps of myogenesis are determined by the expression of the myogenic transcription factors PAX7 (paired box protein 7) [16], MYF5 (myogenic regulatory factor 5), MYOD1 (myoblast determination protein 1), and MYOG (muscle-specific transcription factor myogenin) [17]. Any disturbances to this precisely paced process have substantial effects on muscle homeostasis; consequently, SCs dysfunction is supposed to play a crucial role in the progression of muscle pathology and failed regeneration in various myopathies [18,19].

DMD is one of the most devastating muscle dystrophies in people, an X-linked disease affecting approximately one in 3500–5000 male births and ultimately leading to death in early adulthood [20–22]. It is caused by mutations in *DMD*, the largest known gene in the human genome spanning 2.5 Mb and harboring 79 exons. *DMD* encodes dystrophin, an actin-binding structure protein primarily expressed in skeletal and heart tissue, where it constitutes part of the dystrophin-associated glycoprotein complex (DGC) [23]. The DGC connects cytoskeletal F-actin filaments of the myofiber through the sarcolemma to the extracellular matrix (ECM) and is responsible for muscle fiber integrity and stability. In humans, *DMD* mutations occur mainly in hotspot regions between exons 2 and 10 and 45

Cells 2025, 14, 892 3 of 28

and 55. These mutations are most frequently deletions of one or several complete exons (\sim °60–70%), followed by point mutations (\sim °20%) and exon duplications (\sim °5–15%) leading to a reading frame shift which ablates dystrophin expression [24]. The lack of dystrophin causes instability of the sarcolemma with a rapidly progressing fiber degeneration, which severely compromises the contractile apparatus of the affected muscle tissue [25]. Starting at a young age, affected males show a rapidly progressive muscle weakness leading to walking disabilities, and patients decease in their second or third decade of life due to respiratory and cardiac failure [26,27].

Currently, there are almost 60 different animal models available for DMD research, including mammals (e.g., *Mus musculus*) and non-mammals (e.g., *Caenorhabditis elegans*, *Danio rerio*) [28,29], but when it comes to translational studies, large animal models, reflecting the human conditions most accurately, are of urgent need. On that note, aground great similarities on an anatomical and physiological level to humans, the pig as a pre-clinical model for DMD research has attracted consideration for medical research [30–32]. The first porcine DMD model was developed in 2013 and harbors a *DMD* exon 52 deletion, which leads to a disease phenotype similar to human patients [33]. These models are predominately used for investigations of differentiated, contractile myofibers but offer a great opportunity to expand their application toward research exploring the behavior of dystrophic muscle stem cells.

Motivated by these challenges, we used fresh muscle samples from dystrophindeficient DMD and wild-type (WT) control piglets and optimized current protocols of SCs isolation for use in porcine tissue. Then, free from the influence of the dystrophic environment, enabling the observation of intrinsic cellular changes, we conducted a comprehensive characterization. Isolated cells were analyzed at pre-contractile stages of early muscle development, referring to a state where they have not yet developed the structure or machinery necessary for contraction and prior to the onset of spontaneous or coordinated contraction. To monitor different developmental stages of myogenesis, we analyzed cultivated SCs during proliferation and after induction to differentiate into multinucleated myotubes. After assessing growth capacities and force generation in vitro, we performed bulk RNA sequencing and label-free proteomics to screen for molecular derangements associated with dystrophin deficiency. To find sources explaining the observed variance, we utilized multi-omics factor analysis (MOFA) to integrate transcriptomic and proteomic datasets. We detected increased force generation as well as significantly altered transcriptome and proteome profiles at early and late stages of myogenesis, which unambiguously could be assigned to the lack of dystrophin. We intentionally aimed to capture a broad perspective to identify overarching differences in gene expression patterns without narrowing down the analysis to discrete pathways or molecular events. Our data strongly suggest that dystrophin deficiency indeed highly affects the intrinsic behavior of muscle SCs and impacts myocyte differentiation already at a pre-contractile stage.

2. Materials and Methods

2.1. Tissue Collection

Muscle tissue was procured freshly from 3-day-old male DMD and WT piglets immediately after euthanasia. Upon dissection of overlying tissues, samples of roughly 1.0 cm cube length were taken from *intercostalis* (*INT*) and *pectoralis* (*PECT*) muscles under sterile conditions. The pieces were dipped into 70% ethanol and washed with Dulbecco's phosphate-buffered saline (PBS, GIBCO Thermo Fisher, Schwerte, Germany) supplemented with 1% Penicillin–Streptomycin (PenStrep, GIBCO Thermo Fisher) (PBS+) before being further chopped with a sterile scalpel blade. Fragments of 2–3 mm diameter were stored at 4 °C in DMEM GlutaMax without Pyruvate (GIBCO Thermo Fisher) supplemented with

Cells 2025, 14, 892 4 of 28

20% Fetal Bovine Serum (FBS, GIBCO Thermo Fisher) and 1% PenStrep (DMEM+) until the isolation was performed.

2.2. Isolation of Primary Porcine Satellite Cells

2.2.1. Dissociation of Porcine Muscle Tissue

Working under a sterile laminar flow, muscle biopsies were further minced using a scalpel blade. Attaching connective tissue was grossly removed. Next, the tissue was sterilized again using 70% ethanol, rinsed with PBS+, transferred to a tube containing PBS+ with 1% 1 M HEPES buffer (Sigma Aldrich, Darmstadt, Germany) solution, and centrifuged. The supernatant (SN) was transferred to a new tube and stored on ice (=SN1) until usage. For enzymatic digestion, a protease solution containing 1.5 mg/mL Protease Streptomyces griseus (Sigma Aldrich, 3.5 U/mg), PBS, 1% PenStrep, and 1% 1 M HEPES buffer was added to the tube to completely cover the tissue for a 1 h incubation period at 37 °C. The mixture was agitated by hand every 10-15 min. After the digestion step, the tissue was centrifuged for 5 min at $400 \times g$ and the supernatant (=SN2) was added to SN1. To further dissociate the cells, the mixture was incubated with a collagenase solution consisting of 1 mg/mL Collagenase Clostridium histolyticum (Sigma Aldrich, 800 U/mg), DMEM without Pyruvate GlutaMax, 5% FBS, and 1% PenStrep for 1 h at 37 °C, agitated by hand every 10-15 min. During the second digestion period, SN1 and SN2 were further processed: the suspension was centrifuged for 5 min at $400 \times g$, the supernatant was discarded, and DMEM+ was added. The solution was sifted through a 70-µm nylon strainer (Greiner, Frickenhausen, Germany) and stored on ice until further use (SN3). The digested tissue suspension was filtered through a 70- μ m nylon strainer, centrifuged for 10 min at $400 \times g$, and the cell pellet was resuspended using SN3. The solution was sifted through a 40-µm nylon strainer (Greiner), PBS+ was added to the filtered suspension and the mixture was centrifuged for 5 min at 300× g. The cell pellet was resuspended in DMEM+ and again centrifuged for 10 min at $400 \times g$. The isolated cells were resuspended in DMEM+ and prepared for subsequent purification procedure.

2.2.2. Magnetically Activated Cell Sorting

The heterogeneous cell solution was further processed by magnetically activated cell sorting (MACS) using an indirect labeling approach and two sequential separation steps. First, for depletion of unwanted cells, polyclonal rabbit anti-CD31 (1:200, ab28364, Abcam, Cambridge, UK) and polyclonal rabbit anti-CD45 (1:200, ab10558, Abcam) antibodies were added to the cell suspension in order to bind surface antigens of endothelial, respectively, hematopoietic cells [34] and incubated for 30 min on ice. Subsequently, magnetically conjugated anti-rabbit IgG(-) secondary antibodies (1:15, Miltenyi Biotec, Bergisch Gladbach, Germany) were added and incubated for 30 min on ice. Next, a washing step was performed, and the pellet was resuspended in MACS buffer (Miltenyi Biotec). The MACS separator (Miltenyi Biotec) was placed under the sterile working bench and a LS column (Miltenyi Biotec) was set up on the magnet board with a tube underneath to collect the flow-through. The column was pre-balanced by rinsing with MACS buffer, the cell suspension was transferred into the column, and the solution was gently sifted through by inserting the plunger. The undesired cells were retained in the column by magnetic forces and thus were eliminated from the cell suspension, whereas unlabeled cells flowed through. To target the skeletal muscle satellite cells (SCs) in the remaining solution primary antibodies for monoclonal mouse anti-Integrin-β1 (1:200, ab30388, Abcam), monoclonal mouse anti-NCAM1 (1:200, ab9018, Abcam) and monoclonal mouse anti-M-cadherin (1:200, sc-374093, Santa Cruz, Heidelberg, Germany) [34] and the magnetically conjugated secondary anti-mouse IgG(-) antibodies (1:15, Miltenyi Biotec) were added and incubated

Cells 2025, 14, 892 5 of 28

for another 30 min on ice. Again, a washing step was performed before transferring the solution into a MS column (Miltenyi Biotec) attached to the magnetic board with a tube placed underneath. The column was pre-balanced with MACS buffer and the solution was gently filtered through the column by using the plunger. During this separation step, the desired, magnetically labeled cells remained inside the column due to magnetic forces. Therefore, the flow-through was discarded, a new tube was placed underneath the column, and the tube and column were removed from the magnetic board together. Now, the target cells were eluted by flushing the column with MACS buffer twice. The cell suspension was centrifuged for 3 min at $400 \times g$ and the cell pellet was resuspended in growth medium consisting of Ham's F10 Medium (GIBCO Thermo Fisher), 20% FBS, 1% PenStrep, and $10 \mu g$ recombinant human basic fibroblast growth factor (bFGF, PEPro Tech, Cranbury, NJ, USA). The purified cells were then counted with a Neubauer Chamber and directly seeded on a 10% Matrigel (VWR, Radnor, PA, USA)-coated 12-well plate.

2.3. Primary Cell Culture

After MACS, the cells were incubated in growth medium for 3 days at 37 °C with 5% O_2 uninterruptedly, and afterwards the medium was exchanged every second day. By reaching 70–80% confluency, cells were split using Trypsin/EDTA 0.25% (GIBCO Thermo Fisher) and seeded into 10% Matrigel-coated culture dishes at a concentration of 5000 cells/cm² for all following passages (p). After p3, cells were cultivated in 50 μ g/mL collagen-coated culture dishes using Collagen I, rat tail (GIBCO Thermo Fisher). Differentiation into myoblasts was induced by nutrient starvation using Ham's F10 Medium supplemented with 1% PenStrep and 5% Horse Serum (Biozol, Eching, Germany) for 7 consecutive days, during which the medium was exchanged every second day.

2.4. Traction Force Microscopy

2.4.1. Silicone Substrate Preparation

Employed 60 × 24 mm glass coverslips (Marienfeld, Lauda-Königshofen, Germany) underwent a thorough cleaning process in three steps. Initially, coverslips were sonicated in a 5% v/v solution of Hellmanex III (Sigma Aldrich, Merck) for 10 min, followed by sonication in 1 M potassium hydroxide for another 10 min and, lastly, in 100% ethanol. During each step, the coverslips received a rigorous washing in double-distilled water for 5 min. Finally, compressed nitrogen was used to dry the coverslips. Polydimethylsiloxane (PDMS) substrates were fabricated by combining a 9:10 weight ratio of two components Cy-A and Cy-B from DOWSIL™ CY 52-276 Kit (Dow, Midland, MI, USA), resulting in a substrate stiffness of approximately 12 kPa. The gel solution was mixed thoroughly, centrifuged, and degassed before pipetting 350 µL of the solution onto a glass coverslip. The solution was spin-coated for 90 s using a homemade spinner, with acceleration and deceleration occurring every 30 s, to create a smooth, uniform surface. The gels were cured at 70 °C for 30 min, after which they were stored at room temperature (RT). To functionalize the silicone surface, the gels were treated with a solution of 7% (v/v) 3-aminopropyl trimethoxysilane (APTES) in pure ethanol for 2 h. The gels were washed with pure ethanol, a 1:1 volume ratio of ethanol and PBS, and finally with only PBS, each for three cycles. As a cell culture and imaging chamber, a bottomless 8-well sticky-slide (Ibidi, Gräfelfing, Germany) was mounted on top of each PDMS substrate. After washing the chambers three times with PBS, 100 µL solution of 100 nm, red-orange fluorescent (540/560) FluoSpheres carboxylate-modified microspheres (Invitrogen Thermo Fisher Scientific, Waltham, MA, USA) at a dilution of 1:1000 in PBS was mixed with a final concentration of 100 µg/mL 1-ethyl-3-(3-dimethylaminopropyl)carbodiimide (EDC) and pipetted onto the top surface of the gel containing 200 µL PBS. The solution was incubated for 20 min at RT and washed

Cells 2025, 14, 892 6 of 28

three times with PBS. Next, the gels were coated with a solution of $50\,\mu g/mL$ collagen I with $100\,\mu g/mL$ of EDC in PBS, and incubated for 2 h at RT. After incubating, the chambers underwent multiple washing steps, initially with PBS and then with the cell culture growth medium, before being seeded with cells.

2.4.2. Traction Force Measurements and Data Analysis

To investigate differences in traction forces exerted by the dystrophin-deficient and healthy control SCs, primary porcine SCs derived from 3-day-old DMD and WT piglets were seeded onto the PDMS substrates containing 100 nm fluorescent microspheres at a density of 5000 cells/cm² in growth medium and cultivated under standard conditions for 48 h before performing traction force microscopy (TFM). Fluorescent images of the beads embedded in the PDMS gel were captured at 40× with an inverted IX83 microscope (Olympus, Tokyo, Japan) equipped with a camera (XM10, Olympus) before and after trypsinization the cells using 0.5% Trypsin/EDTA (GIBCO) to obtain pairs of tractionloaded (deformed gel with cells exerting forces onto the substrate) and traction-free (relaxed gel without cells) bead images. We performed further processing and analysis in MATLAB (Version R2020b) with our customized script. The entire analysis workflow includes bead detection and tracking, traction field reconstruction, maximum traction, and strain energy statistical analysis. Fluorescent beads were detected by detectMinEigenFeature, a built-in point detector in MATLAB. Depending on the quality of the image, a difference-of-Gaussian filter with a standard deviation of 1.5 pixels and 2 pixels was applied to suppress background noise and enhance the bead profiles before detection. Bead displacements were then measured by optical flow tracking, which is implemented by vision.pointTracker as suggested by [35]. The tracking window was set to 61 pixels to acquire smooth results. Once the displacement field was generated, traction forces were calculated using Regularized Fourier Transformation Traction Cytometry provided by [36]. All experiments used a constant regularization parameter 2.47×10^{-5} Pix⁻² and the Poison ratio was set to 0.5. For analysis, we collected the maximum traction magnitude within the cell region and strain energy stored in the gel in the current field of view for all experiments and classified the results by different treatments.

2.5. Immunohistochemistry

Formalin-fixed and paraffin-embedded muscle tissue sections from INT and PECT biopsies derived from male DMD and WT were used for immunohistochemistry (IHC) according to standard avidin-biotin peroxidase complex method. After dewaxing and antigen-retrieval, sections were incubated overnight (o/n) at 4 °C with the following primary antibodies: monoclonal mouse anti-PAX7 (1:150, Abcam, ab199010) or polyclonal rabbit anti-Dystrophin (1:100, Abcam, ab15277). The next day, sections were incubated with a biotinylated goat-derived anti-mouse IgG antibody (1:1000, Vector Laboratories, Newark, NJ, USA) or an anti-rabbit IgG antibody (1:1000, Vector Laboratories, BA-1000-1.5) for 1 h at RT, respectively. Subsequently, sections were incubated with a horseradish peroxidase-labeled avidin/biotin complex (1:100, VECTASTAIN Elite ABC-HRP Kit, Vector Laboratories, PK-6100) for 30 min at RT. To visualize immunoreactivity, ImmPACT DAB Substrate Kit (Vector Laboratories, SK-4105) with 3,30-diaminobenzidine tetrahydrochloride dihydrate (DAB) was applied to the sections (brown color). Hemalaun was used for nuclear counterstaining (blue color). For negative control, primary antibodies were omitted and replaced by diluent. Slides were investigated via bright-field microscopy using a Zeiss Axiophot[®] (Zeiss, Oberkochen, Germany) equipped with a CCD camera supported by pylon viewer. For PAX7 quantification, stained sections were scanned with a high-throughput slide scanner (Aperio AT2, Leica Biosystems, Wetzlar, Germany) at

Cells 2025, 14, 892 7 of 28

 $40\times$, and images were taken with Aperio ImageScope (v.12.4.0.7018, Leica Biosystems). Five randomly chosen fields of view with a dimension of approximately 825 \times 450 μm were analyzed by manual counting of PAX7+ cells.

2.6. Immunofluorescence

For immunofluorescence (IF), cells were seeded in a 50 µg/mL collagen-coated 12-well plate containing a coverslip (Neolab, Heidelberg, Germany) and cultivated until reaching 70–80% confluency. Staining was performed in accordance with standard protocols. Briefly, cells were fixed with 4% formalin for 30 min at RT. Next, cells were washed with PBS and blocked with 1% BSA (Carl Roth, Karlsruhe, Germany) and 2.5% NDS (Sigma Aldrich) for 30 min at RT to avoid non-specific binding. The samples were incubated o/n at +4 °C with the following primary antibodies diluted in 1% BSA solution: monoclonal mouse anti-Desmin (1:250, Agilent DAKO, Santa Clara, CA, USA, M0760) or monoclonal mouse anti-PAX7 (1:150, Abcam, ab199010). The next day, cells were washed with PBS and, to reveal primary antibody binding, samples were incubated with the fluorophore-conjugated secondary antibody Alexa Fluor 488 donkey anti-mouse IgG (Invitrogen Thermo Fisher Scientific, Waltham, MA, USA) diluted 1:500 in 1% BSA solution for 30 min at RT. Nuclei were counterstained with Hoechst 33342 (Thermo Fisher Scientific, Waltham, MA, USA) at 1:10,000 for 10 min at RT. Coverslips were mounted on object glass slides (Starfrost; Engelbrecht Medizin- und Labortechnik Gmbh, Kassel, Germany) using Aqua/Poly-Mount (Polyscience, Warrington, PA, USA). Imaging was performed with the Axio Imager Z1.m (Zeiss) equipped with an HBO Lamp (Zeiss) and AxioVision software (Zeiss, Version SE64 Rel. 4.9).

2.7. Immunoblotting

Total cell protein extracts were generated with radioimmunoprecipitation assay buffer (RIPA) containing 1% of 100× Protease/Phosphatase Inhibitor (Cell Signaling, Danvers, MA, USA) according to standard protocols. The protein concentration of each sample was determined by Bradford Assay using the Protein Assay Dye Reagent Concentrate (BioRad, Hercules, CA, USA) as described by the manufacturer, and absorbance was detected with the Infinite F200 Pro plate reader (Tecan, Männedorf, Switzerland) at 595 nm. A total of 25 μg of protein was separated by 6–12% SDS-PAGE and subsequently transferred to polyvinylidene difluoride (PVDF) membranes (Merck Millipore Ltd., Billerica, MA, USA). Next, membranes were blocked using either 1× Roti Block (Carl Roth, Karlsruhe, Germany) or 5% non-fat dry milk (Carl Roth) in Tris-buffered saline (TBS) with 0.5% Tween-20 (Carl Roth) and incubated o/n at 4 °C with the following primary antibodies: monoclonal mouse anti-NCL-DYS1 (1:100, Leica Biosystems), monoclonal mouse anti-NCL-DYS2 (1:100, Leica Biosystems), polyclonal rabbit anti-MYOD (1:500, ProteinTech, Manchester, UK), and monoclonal rabbit anti-β-Actin (1:1000, Cell Signaling, 4970S). The next day, membranes were incubated with horseradish peroxidase-conjugated secondary antibodies goat antimouse IgG (1:5000, Abcam, ab6789) or goat anti-rabbit IgG (1:3000, Abcam, ab6721) for 45 min at RT. For the visualization of protein bands, membranes were incubated with SignalFire ECL reagent (Cell Signaling) as indicated by the manufacturer, and the signal was detected with Amersham Imager 680 (GE Healthcare Amersham, Bioscience, Freiburg, Germany). Semi-quantification of immunoblots was performed using ImageJ (Version 1.54 g) using β -Actin signal as loading control.

2.8. RNA Isolation from Cell Lines, Library Preparation, Sequencing, and Data Analysis

Total RNA from SCs derived from 3-day-old DMD and WT animals was extracted using the NEB Monarch RNA Miniprep Kit. The protocol was performed in accordance with the manufacturer's instructions. To recapture proliferation (PROL) conditions, samples

Cells 2025, 14, 892 8 of 28

were generated at p6 after cultivation in normal growth medium. For the differentiation condition (DIFF), samples were collected after cultivation in differentiation medium containing reduced serum amounts for 10 days at p6. To quantify gene expression in extracted RNA samples, the protocol of 3' mRNA-seq was adapted [37–39]. An amount of 25 ng of total RNA was used, and each sample was analyzed as a technical duplicate. To generate libraries, polyA+ RNAs were selected during cDNA synthesis through annealing to a polydT oligo containing an additional unique molecular identifier (UMI) and a well-barcode, which allowed early pooling of all samples directly after cDNA synthesis., Second-strand synthesis was performed by RT-PCR using a template switch oligo with an integrated Illumina adapter sequence. After purification and exonuclease I treatment, the library pool was amplified by PCR and purified again. To achieve optimal fragment lengths, NexteraXT DNA library prep Kit (Illumina, San Diego, CA, USA) was used. With the Nextera transposon DNA was tagmented, a process that fragments and tags DNA with adapter sequences. For amplification of the library, a 3' enrichment PCR was performed during which i7 and i5 adapters were attached. After purification, the quantity of the library pool (Qubit Fluorometer 4.0, Thermo Fisher Scientific) and average fragment size (LabchipGX Touch 24, Perkin Elmer/Revvity, Waltham, MA, USA) were measured. The resulting library was sequenced on a NextSeq550Dx using a 75-cycle high output kit (Read 1:16° cycle – UMI + barcode; Read 2: 76° cycles – Insert). RNAseq reads were demultiplexed using the program bcl2fastq provided by Illumina. R version 4.1.2 was used for all further analysis. Quality control was performed using the command line tools fastQC [40] and multiQC [41]. Umi-tool dedup [42] was used for deduplication, and the reads were aligned to the Sus scrofa reference genome susScr3 using STAR [43] aligner version 2.7.10b. The number of reads mapping to each gene was also obtained from STAR using the parameter quantMode GeneCounts. edgrR [44] was used for differential expression analysis, and gene set enrichment analysis was performed using fgsea [45].

2.9. Sample Preparation for LC-MS/MS and Proteome Data Analysis

For proteome analysis, SCs from 3-day-old DMD and WT animals were harvested by Trypsin/EDTA 0.25% incubation followed by 5 washing steps with DPBS + 10% PenStrep. Similarly to the approach for RNAseq, cell samples were harvested at two different time points in order to investigate protein expression in PROL and DIFF states: PROL samples were collected at p3 and p6, DIFF samples at p4 and p7. Samples were stored at -80 °C until LC-MS/MS measurements. Using ultrasonication (Sonopuls GM3200, BR30, Bandelin, Berlin, Germany), cells were then lysed in 8 M urea/0.4 M NH₄HCO₃. Protein concentration was assessed photometrically (Pierce 660 nm, Thermo Fisher Scientific). Samples were reduced with dithioerythritol at a final concentration of 5 mM at 37 °C for 30 min and alkylated with iodoacetamide at a final concentration of 15 mM at ambient for 30 min. Protein was digested with lysyl endopeptidase (1:100, enzyme:protein, FUJIFILM Wako Chemicals Europe, GmbH, Neuss, Germany) at 37 °C for 4 h, diluted to 1 M urea with water, and then digested at 37 °C overnight after adding trypsin (1:50, enzyme-protein, Promega, Fitchburg, WI, USA). Samples were then dried and resuspended in 0.1% formic acid in water. For mass spectrometry analysis, 1 µg of peptides was separated and analyzed using an Ultimate 3000 RSLC chromatography system coupled to a QExactive HF-X mass spectrometer (both Thermo Fisher Scientific). For separation, peptides were first trapped on a PepMap 100 C18 trap column at a flow rate of 5 µL/min of 0.1% formic acid in 1% (v/v) acetonitrile in water. Peptides were then separated with an Easy-Spray column $(75 \mu m \times 50 cm; 2 \mu m; both Thermo Fisher Scientific)$ at a flow rate of 250 nL/min with eluent A 0.1% formic acid in water and eluent B 0.1% formic acid in acetonitrile, using a multi-step gradient—initial ramp from 3% eluent B to 6% in one minute, followed by an

Cells 2025, 14, 892 9 of 28

80 min ramp to 20%, followed by a 9 min ramp to 40%. MS spectra were acquired with a top 15 data-dependent method. For protein identification, MaxQuant (Version 2.0.3.0) [46] and the porcine subset of the RefSeq database were used (retrieval date: 5 October 2022). The presented data was analyzed with a label-free quantification algorithm called MaxLFQ, which is part of the MaxQuant software and yields relative quantification values. To account for potential contamination, blank runs between measurements were included, and the protein list was filtered against the MaxQuant built-in contaminant list. For all downstream analyses, only proteins that were detected across all four biological replicates were included.

2.10. Multi-Omics Factor Analysis

MOFA was used to integrate the RNAseq and proteomics datasets. MOFA identifies latent factors (LFs) reflecting the major source of variability across the transcriptomic and proteomic datasets, which are referred to as views. Each factor represents a pattern of variation within the sample and provides a low-dimensional representation of the data, summarizing the underlying biological process (e.g., genotype, phenotype, disease state, developmental condition, etc.) that drives differences between samples. In this way, a factor explains the variance across multiple features, or in our case, across multiple differentially expressed genes and proteins. The factor weight displays how much each feature contributes to a factor, whereas a factor value indicates how strongly a sample expresses the feature pattern.

The model starts with M data matrices $Y_1, ..., Y_m$, each of size $N \times D_m$, where NN is the number of samples and D_m is the number of features in matrix mm. MOFA decomposes these matrices as

$$Y_m = ZW_{mT} + E_m$$
 for $m = 1, ... M$,

Here, Z is the factor matrix common to all data matrices, W_m represents the weight matrices specific to each data matrix mm (also referred to as view mm), and E_m denotes the view-specific residual noise term, which varies depending on the data type.

The model is framed within a probabilistic Bayesian context, applying prior distributions to all unobserved variables. Specifically, a standard normal prior is used for the factors Z, and sparsity priors are applied to the weight matrices W_m [47].

2.11. Statistical Analysis

All data were analyzed with GraphPad PRISM (Version 5.03), Perseus (Version 1.6.7.0) [48], R (R Core Team, Vienna, Austria, Version 2023.06.0), and MATHLAB (Version R2020b). Values are presented as mean and \pm standard error mean (SEM) or standard deviation (SD). To calculate p-values, t-tests, ANOVAs, Tukey Honest Significant Differences, and two-tailed Mann–Whitney U tests were used. The threshold for significant differences was considered as p < 0.05 and significance levels are indicated as p < 0.001 (***), p < 0.05 (*), and p > 0.05 (n.s.). The number of analyzed animals (n) and p-values are listed in the figure legends.

3. Results

3.1. Muscle Sections of DMD Animals Harbor Significantly Elevated Levels of PAX7+ SCs

To verify dystrophin deficiency in Duchenne muscular dystrophy (DMD) tissue, we conducted an immunohistochemical (IHC) staining assay against dystrophin on muscle sections derived from *intercostalis* (INT) and pectoralis (PECT) muscle samples of male DMD (n=6) and wild-type (WT; n=6) animals. As anticipated, dystrophin signal was absent in DMD tissue, whereas in WT, a strong sarcolemma-associated signal was observed.

Cells 2025, 14, 892 10 of 28

There was no obvious difference in dystrophin expression between *INT* and *PECT* sections (Figure 1A, Supplementary Figure S1).

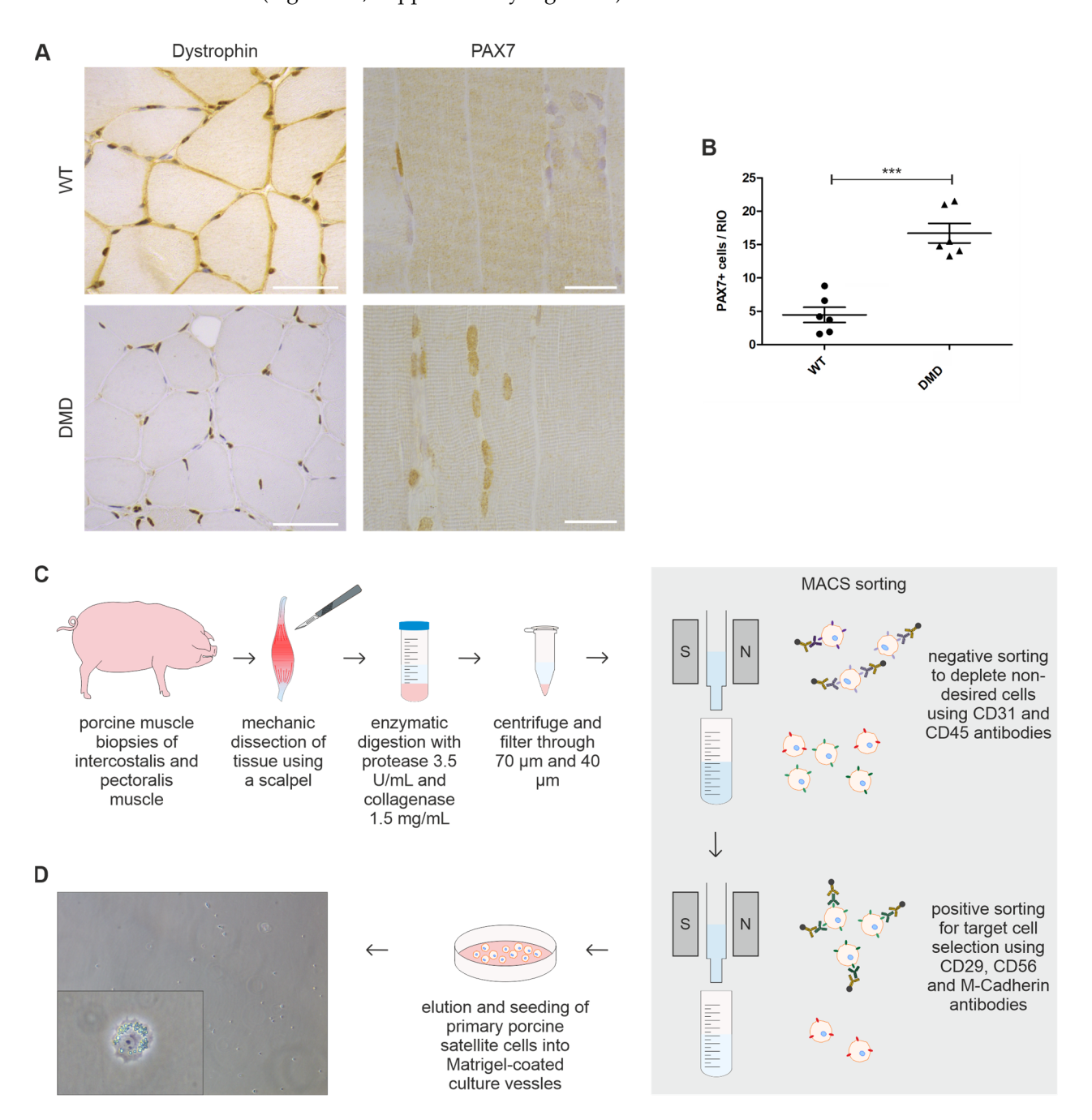


Figure 1. Detection of PAX7+ SC in dystrophin-deficient muscle sections and SCs isolation pipeline. (**A**) Immunohistochemistry of dystrophin and PAX7 in paraffin-embedded PECT muscle sections of DMD and age-matched WT controls. DMD tissue demonstrates absent sarcolemmal dystrophin signal (brown) and high amounts of PAX7+ cell nuclei (brown). Scale bars = 50 μm (dystrophin) and 25 μm (PAX7). (**B**) Significantly higher amounts of PAX7+ cells were detected in DMD (n = 6, triangle, 16.70 ± 1.471) muscle sections when compared to WT (n = 6, dots, 4.467 ± 1.137 ; *** p < 0.001); each dot represents one individual; unpaired t-test was used for statistical testing and results are shown as mean and SEM. (**C**) Schematic overview of isolation procedure of primary porcine SCs derived from INT and PECT muscle biopsies of DMD and WT animals. (**D**) Representative light microscopy pictures of seeded SCs directly after isolation; insert showing magnetically labeled cell. Magnification 10×10^{-1} and 10×10^{-1} and 10×10^{-1} and 10×10^{-1} after isolation; insert showing magnetically labeled cell. Magnification 10×10^{-1} and 10×10^{-1} and 10×10^{-1} and 10×10^{-1} after isolation; insert showing magnetically labeled cell. Magnification

To identify myogenic satellite cells (SCs) and compare the size of the residing stem cell population in muscle sections of DMD (n = 6) and WT piglets (n = 6), we performed an IHC staining against PAX7, a widely used marker for quiescent and early activated SCs [49,50] (Figure 1A). We detected PAX7+ cells at the expected location at the stem cell niche between the sarcolemma and the basal lamina of the muscle fascicle. The quantification of IHC sections revealed that the amount of PAX7+ cells in *INT* muscle of DMD (16.70 \pm 1.471) was 3.7 times higher compared to WT pigs (4.467 \pm 1.137; p = 0.0001) (Figure 1B). Regarding *PECT*, similar results were obtained with a likewise significantly increased number of PAX7+ cells in DMD pigs compared to WT controls.

These results are in line with previous studies detecting higher numbers of PAX7+ SCs in muscle tissue of young mdx mice, a murine model for DMD [6,9,51]. Further, we demonstrate that the increase in PAX7+ SCs is similar in both muscles involved in respiration and movement.

3.2. Isolated PAX7+ SCs from DMD Piglets Lack Dystrophin Expression

To accurately isolate SCs from porcine skeletal muscle biopsies, we developed a modified isolation protocol using a two-step magnetically activated cell sorting (MACS) system with antibodies to deplete undesired cells and to specifically target SCs simultaneously (Figure 1C). A detailed version of our protocol is provided in Supplementary Method S1. Efficacy of the protocol in terms of cell yield and purity of the population was assured by immunofluorescence (IF) staining of cultured cells against desmin, a marker for skeletal muscle intermediate filaments [52,53], and against PAX7. In all samples across the two genotypes, isolated cells presented expression of both markers, confirming the selective isolation of skeletal muscle stem cells (Figure 2A, Supplementary Figure S1). To further investigate the myogenic nature of the cells, expression of the myogenic factor MYOD [54,55] was examined by Western blot analysis of isolated cells harvested in a proliferation state. Both DMD and WT SCs showed a band at approximately 45 kDa corresponding to MYOD protein (Supplementary Figure S1).

To evaluate dystrophin deficiency, the isolated cells were cultured in growth medium and harvested in a proliferative state, and a Western blot analysis using antibodies against the rod domain (DYS1) and the C-terminus (DYS2) of dystrophin was conducted. WT SCs showed a clear band at approximately 427 kDa corresponding to the full-length muscle isoform of dystrophin, as well as one smaller isoform at 268 kDa. In contrast, dystrophin expression was absent in DMD SCs (Figure 2B).

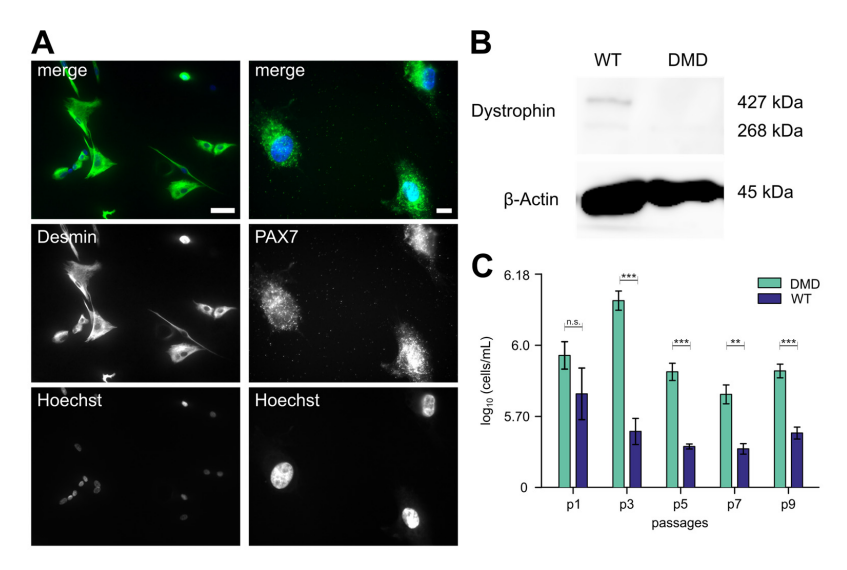


Figure 2. Cont.

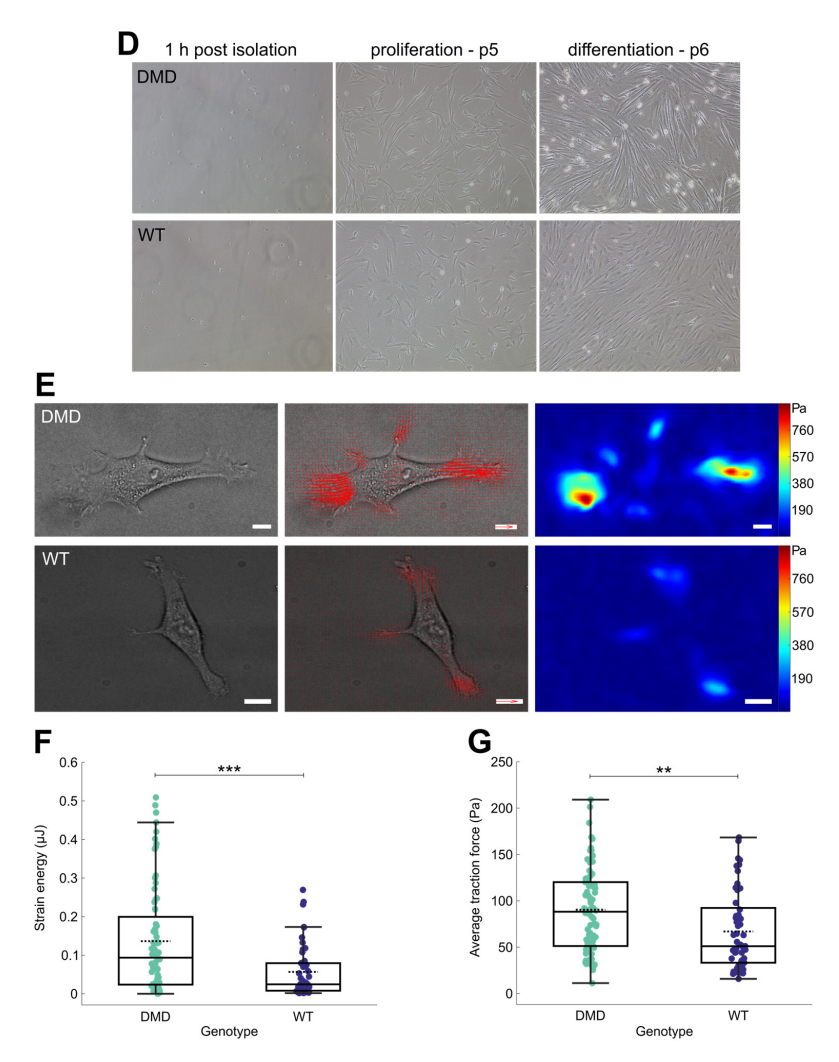


Figure 2. Characterization of isolated porcine SCs and quantification of traction forces in single SC. (A) Immunofluorescence staining of cultured DMD SCs after isolation using desmin (green) and PAX7 (green) antibodies to confirm the cells' identity. Hoechst (blue) was used as a nuclear counterstain. Magnification desmin $20\times$, scale bar = $50 \mu m$. Magnification PAX7 $63\times$, scale bar = $30 \mu m$. (B) Western blot analysis to detect dystrophin expression in DMD and WT SCs lysates. A band at approx. 427 kDa indicates dystrophin expression in WT cells, which is completely absent in lysates of DMD cells. β -Actin was used as loading control. (C) Amount of \log_{10} (cells/mL) for DMD (n = 4, green) and WT (n = 4, purple) over the span of 9 passages (p) in vitro; values are displayed as mean and SEM, n.s. not significant, ** p < 0.01, *** p < 0.001. (D) Representative bright-field pictures of primary porcine SCs culture in vitro 1 h post isolation, during proliferation at p5 and after serum withdrawal to induce differentiation at p6. Magnification 10×. (E) Representative bright-field images of DMD and WT SCs (left) in p7, with corresponding traction force vector (quiver) plots (middle) and traction force magnitude maps (right). In the quiver plots, red arrows indicate the direction and relative magnitude of traction forces exerted by the cells; the reference arrow corresponds to 1 kPa. The color-coded traction map displays force magnitudes in Pascals (Pa), with red indicating high traction stress and blue representing low or negligible force. Areas without cells appear blue, reflecting the absence of measurable traction. Force hotspots typically align with regions of strong cell–substrate interaction, such as focal adhesion sites; scale bar = $10 \mu m$. (F) Strain energy (DMD, green, 72 cells, $0.136 \pm 0.016 \mu$ J; WT, purple, 50 cells, $0.057 \pm 0.008 \mu$ J, *** p = 0.00052) and (G) average traction force levels (DMD 90.391 \pm 10.508 Pa; WT 66.948 \pm 8.867 Pa; ** p = 0.0018) visualized as box plots overlaid with swam charts; each dots represents one cell; two-tailored Mann-Whitney U test was used for statistical testing and results are presented as mean \pm SEM.

These data show that our protocol allows the isolation of porcine myogenic SCs and lend proof of failed dystrophin expression in DMD SCs; thus, we decided to use the cells for all subsequent experiments in this study.

3.3. DMD SCs Morphology Under Proliferation and Differentiation Conditions

Following MACS isolation, SCs were seeded into Matrigel-coated culture vessels and SCs from both DMD and WT animals uniformly started to adhere within 12 h (Figure 1D). In this period the cells of both genotypes displayed a small, round shape with a diameter of approximately 5–10 μm. Upon adherence, the cells successively increased in length and volume and displayed a clear cytoplasm with a prominent nucleus. After 3-4 days in culture, the cells presented with typical arborized, stellate myoblast morphology with several extending processes (Figure 2D). Proliferating SCs were cultivated in standard growth medium until reaching °70–80% confluence. Thereafter, the cells were passaged every other day and manually counted to estimate cell numbers. Throughout nine passages (p), we observed significant differences between cell numbers of DMD (n = 4) and WT SCs (n = 4). DMD numbers peaked at p3 and declined slightly until p9. In contrast, cell numbers of WT SCs were highest at p1, then steadily decreased and maintained roughly the same level (Figure 2C). To induce differentiation in DMD and WT SCs, we performed serum deprivation for 10 days. On day 4 of serum reduction, the cells of both groups increased in length and displayed an elongated, bipolar shape. Aligned, multinucleated myotubes were observed on day 6 (Figure 2D). During the following days, myotubes continued to grow in size and further fused. Microscopic examination revealed no major differences in cell morphology between DMD and WT myotubes.

3.4. DMD SCs Exhibit Increased Force Generation

To investigate how dystrophin deficiency affects force generation and contractility in SCs, we employed traction force microscopy (TFM). We seeded the cells onto poly-dimethylsiloxane (PDMS) substrates with a Young's modulus of approx. 12 kPa, which closely mimics the physiological stiffness of muscle tissue [56]. A single layer of fluorescent nanospheres was embedded on the substrate surface to enable precise force measurements. To quantify the magnitude of the mechanical forces that cells exert on their surrounding environment, we measured the displacement of the beads within the substrate and subsequently calculated traction forces fields using standard Bayesian Fourier Transform Traction Cytometry (Figure 2E). We observed that the strain energies generated by individual cells were, on average, significantly higher for DMD SCs (n = 4, 72 cells overall, 0.136 \pm 0.016 μ J) than for WT SCs (n = 4, 50 cells overall, 0.057 \pm 0.008 μ J; p = 0.00052) (Figure 2F). Additionally, exerted average traction forces were significantly higher for DMD (90.4 \pm 10.5 Pa) than for WT SCs (66.9 \pm 8.9 Pa; p = 0.0018) (Figure 2G). The uneven number of analyzed cells between the genotypes reflects data quality filtering, not sampling bias, since we retained only cells for analysis that met the criteria for reliable traction analysis.

Thus, dystrophin deficiency in muscle SCs influences force generation already at a level of individual cells, which highlights its significance to the pathological characteristics of DMD, which in turn could affect cell-ECM interactions and mechanotransduction [23].

3.5. Overview of Transcriptome Profiles of DMD and WT SCs

To obtain insight into the effects of dystrophin deficiency on the transcriptome of SCs in a proliferative state (PROL) as well as during differentiation into myotubes (DIFF), RNA isolated from DMD (n=4) and WT (n=4) SCs samples were analyzed by 3' mRNA-seq (adapted from [37–39]). We performed preliminary experiments to compare SCs from INT and PECT muscles and did not detect differences. Based on this observation, we focused the extensive omics investigation on SCs derived from INT muscle only. Principal

Cells 2025, 14, 892 14 of 28

component analysis (PCA) clearly separated the transcriptome profiles of DMD SCs and WT SCs, both at the PROL and DIFF states, in the first two principal components (PC1 and PC2) (Figure 3A). Unsupervised hierarchical clustering further confirmed the genotypeand state-dependent separation of transcriptome profiles (Figure 3B).

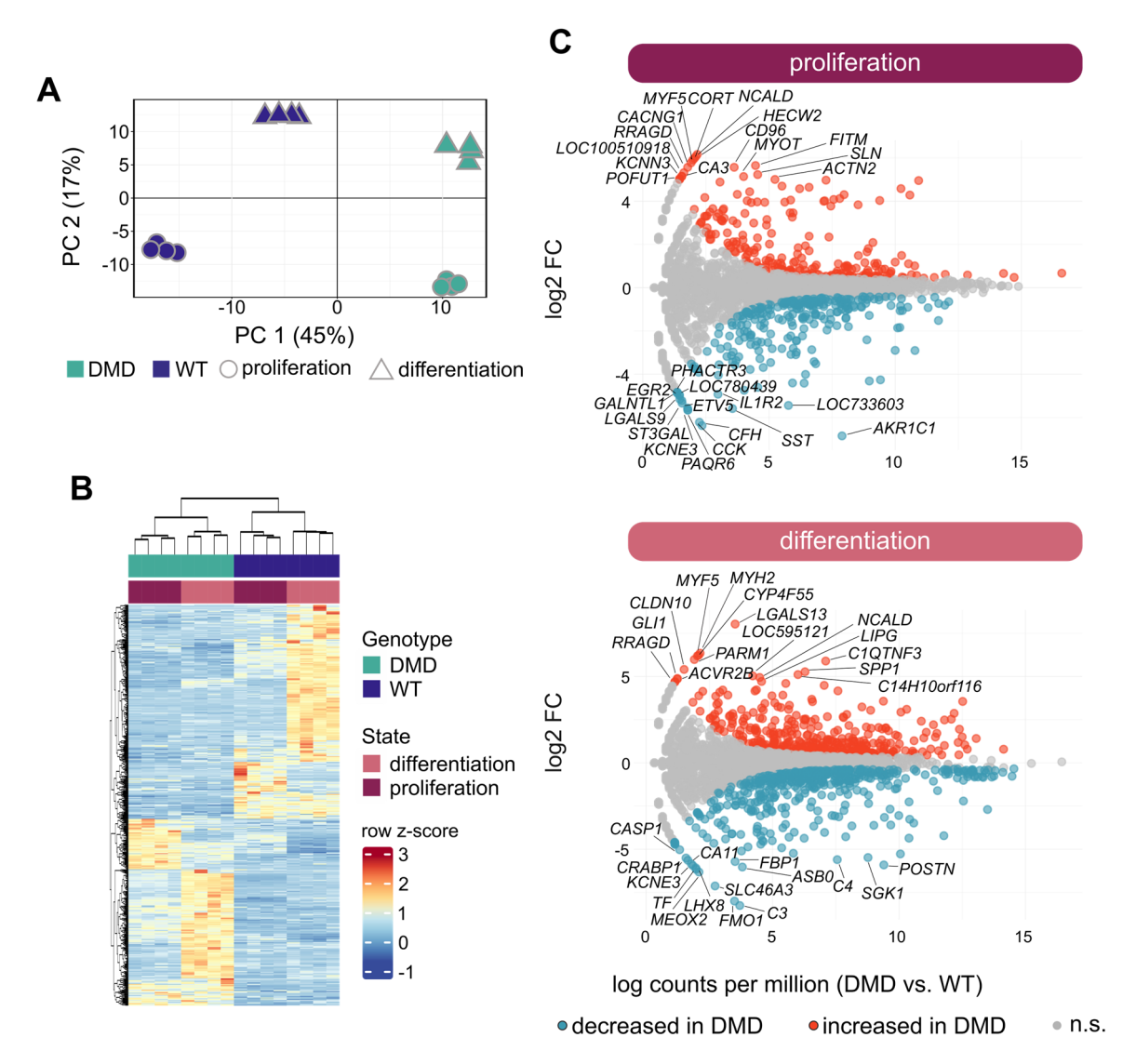


Figure 3. Transcriptome analysis of DMD and WT SCs. **(A)** Principal component analysis of the transcriptome profiles of SCs derived from DMD (n = 4, green) and WT (n = 4, purple) piglets in proliferation (dots) and differentiation (triangles) state; each symbol represents one individual. The percentage of variation in each component is indicated. **(B)** Heat map generated by unsupervised hierarchical clustering of the top 500 differentially expressed genes between DMD and WT SCs. **(C)** Total number of differentially expressed genes between DMD and WT (p-value < 0.05, $|\log 2|$ fold change |>0.6) displayed as MA plot for proliferation and differentiation state, red color indicates upand blue color downregulated genes in DMD SCs; genes are represented as dots, n.s. not significant.

These findings emphasize that dystrophin deficiency could indirectly play a role in the regulation of gene expression in yet undifferentiated states of muscle development.

3.6. Transcriptional Changes in DMD SCs Analyzed in Proliferative and Differentiated States

In the PROL state, we identified 568 differentially expressed genes (adjusted p-value < 0.05; $|\log 2|$ fold change |>0.6) between DMD and WT SCs (261 with higher and 307 with lower expression levels in DMD). Amongst genes showing the strongest upregulation in DMD, we detected HECW2, NCALD, CORT, and several key myogenesis

Cells 2025, 14, 892 15 of 28

genes, including *MYF5*, *MYOD1*, and *MYOG*., The top-downregulated genes included *AKR1C1*, *CFH*, *CCK*, and *PAQR6* (Figure 3C). Using the DAVID online tool, we conducted a gene ontology (GO) enrichment analysis using the biological process (BP) database. Upregulated genes in DMD SCs showed a significant enrichment of gene sets related to skeletal muscle fiber development, sarcomere organization, skeletal muscle contraction, and positive regulation of myoblast differentiation. On the other hand, the top-downregulated genes in DMD SCs were associated with the ontologies of inflammatory response, positive regulation of angiogenesis, response to hypoxia, cell migration, and adhesion.

Analyzing the DIFF state, we detected 822 differentially expressed genes (adjusted p-value < 0.05; $|\log 2$ -fold change |> 0.6) between DMD and WT SCs (391 with higher and 431 with lower expression levels in DMD). Genes displaying the strongest increase in expression in DMD SCs were LGALS13, MYF5, and MYH2. Additionally, the mRNA levels of smooth muscle-related genes like TAGLN and CNN1, as well as myosin light chain genes MYLPF and MYL1, were increased. The latter two were also strongly increased in the PROL state (see above). Interestingly, elevated transcript levels of the myogenic transcription factors MYF5 and MYOG were identified. The top-downregulated genes in DMD SCs comprise C3, FMO1, and SLC46A3. (Figure 3C). The GO-BP analysis revealed that the top-upregulated genes in DMD SCs displayed a significant enrichment of gene sets associated with muscle contraction, apoptotic process, and glycolytic metabolism. Amongst the top-downregulated genes in DMD SCs, we identified significant enrichment of gene sets related to the ontologies of cytoplasmic translation, negative regulation of cell growth, response to oxidative stress, and TGF-β signaling pathway. A detailed list with differentially expressed genes and identified pathways is provided in Supplementary Tables S1-S4.

Collectively, these data highlight the diverse role of dystrophin at different stages of myogenesis and show that dystrophin deficiency affects a broad spectrum of intracellular processes ranging from myoblast-specific pathways to universal cell signaling cascades.

3.7. Overview of the Proteome Profiles of DMD and WT SCs

To achieve a comprehensive overview of the consequences of dystrophin deficiency in SCs, we performed quantitative proteomics using liquid chromatography tandem mass spectrometry (LC-MS/MS) with DMD (n = 4) and WT SCs (n = 4) in PROL and DIFF states, aiming to explore any molecular alterations on the protein level between the genotypes in the different developmental stages.

In total, 49,115 peptides were identified, which could be assigned to 4297 proteins at a false discovery rate (FDR) of 1%. In all samples, characteristic markers for skeletal muscle tissue were detected, namely sarcomere-associated myosin heavy and light chain proteins (e.g., MYH9, MYL6, MYH3) and actins (e.g., ACTG1, ACTA2), contraction-related tropomyosins (e.g., TPM1, TPM4, TPM3), as well as the muscle-specific intermediate filament desmin (DES). A list of all identified and quantified proteins can be found in the Supplementary Tables S5 and S6.

The dimensionality of the proteomic data was reduced using PCA, showing a separation of the proteome profiles of DMD and WT SCs in both the PROL and DIFF cell states (Figure 4A), which is in line with the findings of the transcriptome analysis. Notably, unsupervised hierarchical clustering of DMD and WT SCs in DIFF and PROL states did not separate the groups according to genotype and state but revealed two major clusters. One cluster consisting of only WT DIFF and a second cluster composed of WT PROL, DMD PROL, and DMD DIFF (Figure 4B). This finding demonstrates that DMD SCs' proteomes are more similar to WT PROL than WT DIFF, indicating impaired differentiation in DMD SCs.

Cells 2025, 14, 892 16 of 28

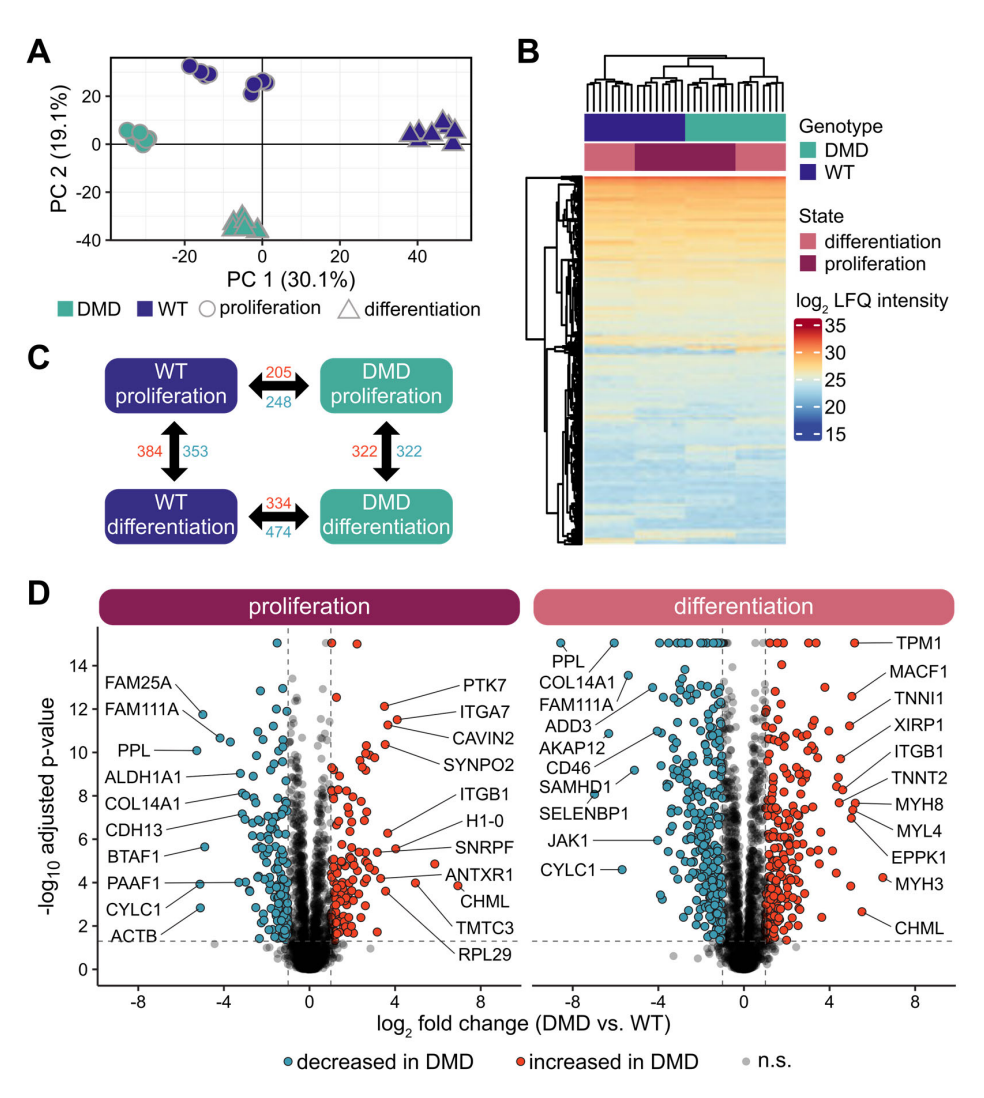


Figure 4. Proteome analysis of DMD and WT SCs. (**A**) Principal component analysis of the proteome profiles of SCs derived from DMD (n = 8, green) and WT (n = 8, purple) animals in proliferation (dots) and differentiation (triangles) state; each dot represents one individual. The percentage of variation in each component is indicated. (**B**) Heat map and unsupervised hierarchical clustering of protein intensity values from proteome expression profiles of DMD and WT SCs. (**C**) Differentially abundant proteins within (horizontal) and between (vertical) DMD and WT SCs proliferation (vertical) and differentiation (horizontal) state. Numbers of proteins with significantly higher (red) and lower (blue) abundance with an adjusted p-value of <0.05 and a |log2 fold change| > 0.6. (**D**) Volcano plots of differentially abundant proteins between DMD and WT SCs in proliferative or differentiated state—two-way ANOVA followed by Tukey Honest Significant Differences was used for statistical testing; as significance cut off adjusted p-value < 0.05 and log2-fold change >0.6/<-0.6 was used. Proteins are represented as dots; red color indicates higher and blue lower abundance in DMD cells, n.s. not significant.

Proteomic profiling of DMD and WT SCs highlights the complexity of DMD myopathology and points towards a highly altered molecular profile of DMD SCs along the myogenic pathway.

3.8. Changes in Protein Expression in DMD SCs Analyzed in Proliferative and Differentiated States

By further statistical analysis, we detected proteins with significantly altered abundances between DMD and WT SCs (adjusted p-value < 0.05; $|\log 2|$ fold change |> 0.6). Analyzing DMD and WT SCs in PROL state, we identified 453 proteins significantly altered

Cells 2025, 14, 892 17 of 28

in abundance (205 with increased and 248 with decreased abundance in the DMD samples). Amongst proteins with the highest increase in abundance, we found ITGA7, ITGB1, DES, and TPM1, whereas among the strongest decrease in abundance proteins included PPL, ACTB, and MYH11. In the DIFF state, the number was even higher, with 808 differentially abundant proteins (334 with increased and 474 with decreased abundance in the DMD samples) (Figure 4C). Top differentially expressed proteins included several myosins (MYH3, MYH8, MYL4, MYL11), troponins (TNNI1, TNNT2, TNNC1), and MACF1 with higher and PPL, CYLC1, ALDH1A3, and ALDH1A1 with lower abundance.

Using DAVID on the differentially abundant proteins, we investigated several functional GO categories, such as biological process, cellular component, and molecular function, as well as the Kyoto Encyclopedia of Genes and Genomes (KEGG) database. In PROL, clusters of proteins with increased abundance in DMD compared to WT showed significant enrichment in proteins related to mRNA splicing, ribosome/translation, structural constituent of cytoskeleton, DNA replication, and focal adhesion. Sets of proteins with decreased abundance in DMD were related to GTP binding, biosynthesis of nucleotide sugars, and regulation of cytoskeleton. At the DIFF state, proteins with higher abundance in DMD SCs were associated with the regulation of actin cytoskeleton, ribosome, hypertrophic cardiomyopathy, and pathways of neurodegeneration. Analyzing proteins of lower abundance in DMD SCs, we detected a significant enrichment in protein sets corresponding to GTPase activity, biosynthesis of nucleotide sugars, microtubule cytoskeleton, proteoglycans in cancer, and aldehyde dehydrogenase activity. Changes in protein abundance are displayed as Volcano plots in Figure 4D. A detailed list of differentially abundant proteins can be found in Supplementary Tables S7 and S8.

Apart from changes caused by the lack of dystrophin between the genotypes, we found state-dependent alterations within the genotype. In DMD SCs, 578 proteins were significantly altered in abundance (256 with increased and 322 with decreased abundance) in DIFF compared to PROL state, and in WT SCs, 737 proteins were differentially abundant (384 with increased and 353 with decreased abundance) in DIFF compared to PROL state (Figure 4C).

In conclusion, we discovered various new factors that are subject to regulation by dystrophin deficiency on a protein level, and our data further reiterated the high degree of proteome alterations in dystrophin-mutated individuals.

3.9. Integration of Transcriptomic and Proteomic Data

In our study, we used MOFA on the transcriptome and proteome dataset to find factors that account for the variability between DMD and WT SCs and characterized the features that contribute to these factors. The cumulative contribution to the variance was 61.95% from the transcriptomic and 54.02% from the proteomic dataset (Figure 5A). We identified five factors explaining the variance between DMD and WT SCs. Within these factors, factors 1 and 2 explain the highest percentage of variance in both -omics datasets, with factor 1 accounting for 31.33% and 32.30% and factor 2 for 23.63% and 15.03% in gene and protein expression variability, respectively (Figure 5B). Factor 1 discriminated against the WT PROL and DIFF from DMD PROL and DIFF, while factor 2 separated the samples into WT DIFF and DMD DIFF from WT PROL and DMD PROL (Figure 5C). The top 25 features for factors 1 and 2 in transcriptomic and proteomic modality with their sample expression can be found in Supplementary Figure S2. Heat maps for factor 1, which distinguished DMD from WT SCs, showed two major clusters in both -omics modalities: one consisting of only WT DIFF and a second one with DMD PROL, DMD DIFF, and WT PROL (Figure 5D–G). This finding recapitulates our previous observation on the proteomic profiles of the DMD and WT SCs. Heat maps for factor 2, which separated PROL from DIFF cells, revealed

that this separation is more driven by the transcriptomic dataset, whereas in the proteomic view, the DMD DIFF samples clustered apart from the rest of the samples (Figure 5C,D). When performing GO enrichment analysis for the top positive factor 1 weights (more abundant in WT), enriched pathways were autophagy, immune response, response to hypoxia, and cell differentiation in the transcriptome data, while protein transport, ER to Golgi vesicle-mediated transport, and actin cytoskeleton organization were enriched in the proteome data. Top negative factor 1 weights (more abundant DMD) were associated with cell cycle and division, sarcomere organization, muscle contraction, and homeostasis in the transcriptome data and translation, mRNA splicing, and ribosome assembly in the proteome data. GO enrichment analysis for top positive factor 2 weights (more abundant in DIFF) in the transcriptome revealed processes related to metabolism, G protein signaling, and response to insulin, while in the proteome layer, pathways of fatty acid biosynthesis, mitochondrial ATP synthesis, and response to oxidative stress were enriched. Top negative factor 2 weights (more abundant in PROL) were associated with protein folding, translation, and cell cycle transition in both -omics modalities.

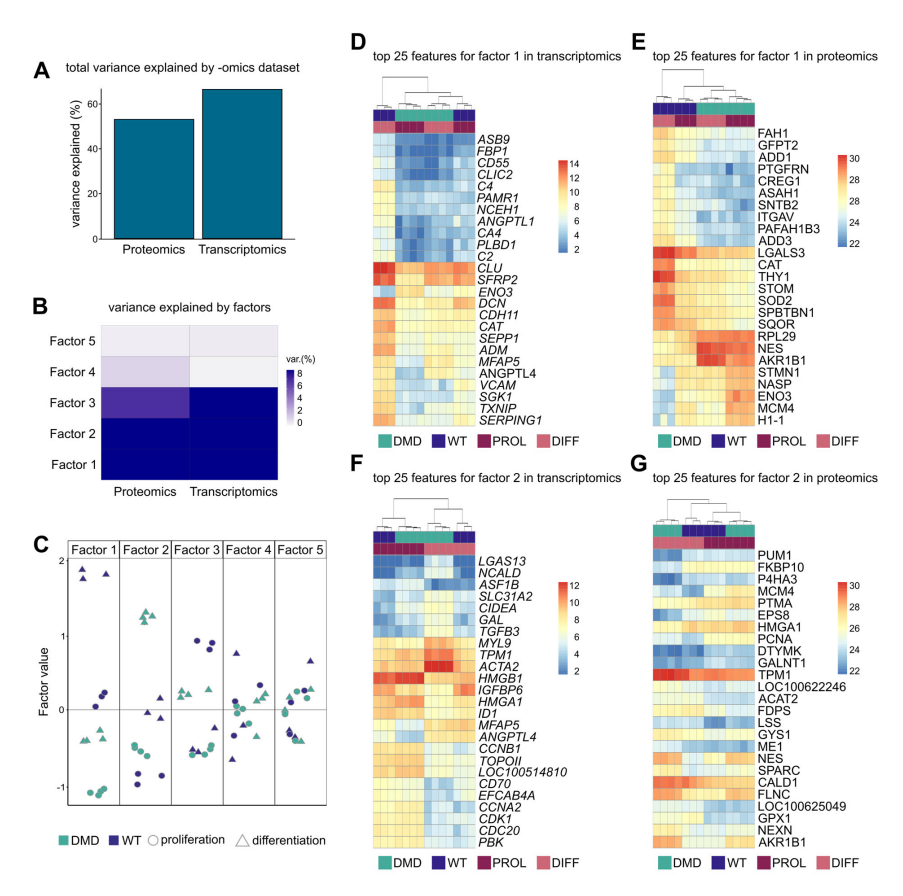


Figure 5. Multi-omics factor analysis of transcriptome and proteome of DMD and WT SCs. (**A**) Cumulative variance explained by each -omics modality in percentage. (**B**) Percentage of variance explained by factors identified by multi-omics factor analysis within the transcriptomic and proteomic data. Higher percentages of variance among the -omics layers indicate a higher amount of shared variability. (**C**) Swam plot of factor values reveals clustering of DMD (n = 4, green) and WT SCs (n = 3, purple) in proliferation (dots) and differentiation (triangles); each dot represents one individual. (**D**) Top 25 features contributing to factor 1 from transcriptomic and (**E**) proteomic data. (**F**) Top 25 features contributing to factor 2 from transcriptomic and (**G**) proteomic data. Heat maps display the distribution of the features across the samples.

4. Discussion

For the last two decades, tissue research in DMD has focused on the pathology of the mature myofiber, investigating sarcolemma weakening, myofiber necrosis, muscle atrophy, myofibrosis, and inflammation in contractile stages of muscle development [57]. The discovery of dystrophin expression in murine SCs [1] provided new insights into the pathophysiology of DMD, and recent studies explored the association of diminished regenerative capacity in dystrophin-deficient SCs. However, the origin of these deficiencies remains unclear; in particular, it is still not fully understood if these deficits result from the surrounding pathologic stem cell niche or if they emerge from intrinsic cell properties.

In this study, we showed that SCs derived from a porcine model of DMD present highly altered intrinsic cellular characteristics. We monitored significantly higher traction forces exerted by the DMD SCs on their substrate. This observation hints towards modified cytoskeleton-ECM interactions in dystrophin-deficient SCs, causing alterations in mechanotransduction of cellular responses to external stimuli, which in turn could impact internal signaling pathways. Gene and protein expression analysis revealed highly altered profiles of isolated DMD SCs compared to their healthy counterpart. We detected dysregulation of major myogenic transcription factors, indicating a disrupted regeneration capacity that could contribute to the impaired muscle regeneration observed in DMD pathology. Collectively, our data indicate that dystrophin deficiency has a direct impact on the perturbed phenotype of DMD SCs, accounting for the observed differences from healthy SCs. This initial defect likely results in secondary effects triggered by indirect consequences, such as altered signaling or microenvironment interaction, further contributing to SC dynamics in DMD.

Due to great similarities with human anatomy, physiology, and metabolism [58], the use of porcine models to generate clinically relevant data is particularly favorable. The DMD pig, which was characterized extensively by Stirm et al. [59], represents a suitable model for DMD research, reflecting the main pathologic features observed in human patients, and has greatly enriched disease understanding. In contrast to human samples, porcine muscle biopsies are accessible at young ages, including fetal stages, which allows monitoring of early—even pre-natal—disease events. Standardized procedures and systematic sampling from homogenous age- and/or stage-matched groups of DMD-affected animals ensure sample quality, which is difficult to achieve in human patients' samples. It should be acknowledged, however, that the DMD pig represents a valuable model; inherent species-specific differences inevitably exist, and careful consideration is required when translating results to humans. For our study, we chose biopsies of dystrophin-deficient and WT INT and PECT muscle tissue due to their relevance and complementary roles in DMD pathology [60,61]. *INT* is crucial for respiratory functions, whereas *PECT* is mainly responsible for upper limb movement. This combination allows the assessment of disease effects on life-sustaining and movement muscles. Additionally, the *INT* muscle is often used in *mdx* mouse studies, enabling cross-species comparisons. The use of porcine DMD muscle biopsies for SC isolation offers the possibility to investigate the intracellular effects of dystrophin deficiency in SC pathogenesis, unaffected by the dystrophic niche. Despite higher costs, more intensive care, and stricter ethical regulations compared to rodent models [62,63], porcine tissue allows the generation of large pools of SCs, thereby reducing the number of animals needed. By using the MACS system in our study, we were able to isolate a high number of viable cells for extensive characterization [64]. Cultivating SCs in vitro offers the chance to monitor DMD implications along the myogenic pathway since SCs can be induced to differentiate in a controlled and reproducible manner [65,66]. To minimize the non-negligible disadvantages of phenotypical changes occurring in primary cell cultures at the time of cultivation [67], we limited our experiments to cells only up to

Cells 2025, 14, 892 20 of 28

p7. We used bulk RNAseq and label-free proteomic measurements to comprehensively investigate the transcriptomic and proteomic profiles of isolated SCs, as these approaches allow a robust, quantitative assessment of global expression patterns [68]. While these techniques do not resolve cellular heterogeneity or capture low-abundance proteins as sensitively as single-cell or targeted approaches [69,70], we considered them suited for our aim of broad, unbiased characterization of molecular alterations in the DMD SC population. To summarize, the use of SCs offers a feasible system for basic research experiments and genetic manipulations for preclinical studies, drug testing, protocol optimization, and therapeutic approaches.

Using Western blotting, we detected dystrophin expression in WT SCs, whereas it was absent in the dystrophic counterpart, pointing towards a direct function in muscle stem cells rather than solely accounting for the structural deficiency of the mature myofiber. Already in 1983, it was hypothesized that undifferentiated DMD myoblasts exhibit intrinsic abnormalities [71], which was discounted soon after [72], and over the next years, researchers explained the altered SC phenotype by an indirect effect of the dystrophin deficiency. However, recent reports on dystrophin-deficient murine and patient-derived myoblasts are now calling this hypothesis into question by reporting major transcriptomic and functional changes in proliferation, chemotaxis, and differentiation, which are maintained even after long-term cultivation [5,73,74]. Notably, comparison of key alterations in mouse and human DMD myoblasts revealed great consistency. In line with these findings, we showed through extensive transcriptomic and proteomic profiling that dystrophin deficiency in porcine DMD SCs triggers a broad range of functional, cell-autonomous abnormalities, which are a direct consequence of the absence of dystrophin in the undifferentiated stem cell state. As a next step, comparative analyses of porcine, murine, and human datasets will be essential to identify cross-species specific similarities and differences to elucidate conserved mechanisms in DMD pathology.

PAX7 is an important regulator of stem cell maintenance conserved in several species and is widely used as a SC marker [50,75]. By PAX7 IHC, we examined the number of residing SCs in muscle sections of DMD and WT piglets and detected significantly higher amounts of subsarcolemmal PAX7+ cells in DMD tissue compared to controls. This is consistent with other studies where higher levels of SCs were observed in muscle tissue of mdx mice [8] as well as in human DMD patients [6]. Dystrophin is implied to be involved in cell polarity formation by binding MARK2, an essential component of cell polarity. Dystrophin-deficient SCs fail to establish a proper apico-basal orientation of regulatory proteins, which affects asymmetric cell division. In turn, this favors stem cell self-renewal over the production of progenitor cells for muscle restoration, thus explaining the increased amounts of PAX7+ SCs along with a reduced regenerative capacity observed in DMD muscle [1,76]. Restoring cell polarity as a potential therapeutic intervention could promote asymmetric division in SCs and enhance muscle repair in DMD patients [12,77]. Interestingly, in our study, we found a similar increase in PAX7+ SCs in INT and PECT muscle sections of DMD piglets compared to controls. In this regard, it seems that the mechanisms in life-sustaining muscles are similar to those for locomotion, and treatment strategies to support muscle regeneration could act on several muscle groups.

In muscle tissue, dystrophin mechanically connects the cytoskeleton's F-actin filaments to ECM proteins, thus contributing to stability and integrity of the cell membrane [78]. In that way, it has been hypothesized that dystrophin alters focal adhesion tension and is successively involved in force transmission and mechano-signaling between the cell and its surroundings [23]. By applying TFM, we found that dystrophin-deficient SCs generated significantly higher strain energy levels and average traction forces. In a recent study, a similar observation was made on immortalized cells from human DMD patients, which dis-

Cells 2025, 14, 892 21 of 28

play higher traction forces than their healthy counterparts [79], highlighting the relevance of our porcine model for translational research approaches. Higher traction forces in SCs could reflect a modified interaction between the cells and the ECM, leading to alterations in the generation and response to mechanical signals that may influence signaling pathways related to proliferation and differentiation [80]. Modified cell-ECM interaction could also influence effective adhering, which alters the mechanical properties of the tissue, changing stiffness and elasticity of the muscle [81]. Furthermore, tissue remodeling is considered another consequence of a modified cell-ECM interplay [82,83]. Increased secretion of pro-fibrotic factors by SCs [84], which directly contributes to the eminent DMD feature of fibrosis, the extensive deposition of ECM-proteins like collagens substituting muscle with fibrotic tissue [85], could therefore be linked to the altered mechanical properties observed in our study. Controversially, another recent publication reported lower focal adhesion tensions in a dystrophin-deficient C2C12 myoblast model [86]. An explanation for these contradictory results could be the differences in stiffness of the substrate: while Ramirez et al. used 4.6 kPa gels, others and we cultivated the cells on 12–15 kPa gels mimicking the physiological stiffness of muscle tissue [56,87].

By RNA-seq analysis, we revealed a heterogeneity of transcriptional dysregulations in DMD SCs. Whole expression profiles separated in a genotype- and stage-specific manner, reflecting a high diversity in transcriptomes between DMD and WT SCs. Amongst genes with the highest differential expression levels, we identified key myogenic transcription factors MYF5, MYOD1, and MYOG, which are indispensable for orchestrating myogenesis in SCs [54]. In particular, in proliferating DMD SCs, increased levels of MYF5, a key factor for promoting and maintaining proliferation in muscle progenitor cells [88,89], are noteworthy. Elevated MYF5 expression could point towards a hyperproliferative behavior of dystrophin-deficient SCs, which in turn perturbs the progression along the myogenic differentiation pathway. In healthy myoblasts, several sarcomeric transcripts are already expressed before fusion into myotubes to ensure proper assembly of a functional contractile apparatus in mature muscle tissue [90]. We found upregulated genes related to sarcomere organization and contraction in proliferating DMD SCs, which could indicate a compensatory mechanism for enhancing muscle function. Further examinations of this finding are necessary, especially because we observed higher traction forces in DMD SCs, and sarcomeric components are essential for producing the contractile, force-generating units of muscle cells. On the other hand, significantly decreased transcript levels in proliferating DMD SCs include hypoxia-associated factors. In healthy SC, hypoxia enhances differentiation in a HIF1 α -dependent manner [91,92]. Alterations in transcript levels of hypoxia-related genes could thus hamper this response and impair myogenesis in dystrophin-deficient SCs.

Gaining deeper insights into the molecular consequences of dystrophin deficiency through proteome analysis, we found a clear separation of the WT DIFF cells from the rest of our cohort, indicating a highly impaired differentiation behavior of the DMD SCs. The number of differentially abundant proteins in DMD DIFF almost doubled compared to the PROL counterpart, further emphasizing the fundamental impact of dystrophin deficiency on protein composition during myogenesis. In proliferating DMD SCs, focal-adhesion-associated integrins ITGB1, ITGA7, and ITGA6 were more abundant than in the corresponding WT SCs. Integrin-based adhesion sites are largely responsible for force transmission between intra- and extracellular compartments [93] and co-localize with the dystrophin-glycoprotein complex at the sarcolemma [94]. It has been suggested that the physical proximity of the two systems implies a mutual regulation of transmitted forces and signals [95]. In this way, increased integrin expression could be an explanation for the elevated traction forces observed in DMD SCs in this study. Future studies should investigate this aspect further to avoid potential oversimplification since traction force

Cells 2025, 14, 892 22 of 28

generation is a multifactorial process involving cytoskeleton, cell-ECM interactions, and external stimuli. In a recent publication, it was demonstrated that isoforms of the ALDH enzyme family are essential for myogenic differentiation [96]. In our analysis, we detected reduced amounts of ALDH1A1 and ALDH1A3 in differentiated DMD SCs. This reduction could contribute to the disturbed differentiation behavior in dystrophin-deficient SCs and should be validated in future investigations.

Using MOFA, a technique that allows the combined analysis of several omics datasets to explain the variability observed across samples [97], we captured multi-layered effects of dystrophin deficiency in SCs. We detected an overall slightly higher contribution of the transcriptomic than the proteomic data to the observed variance between WT and DMD SCs. The lower proteomic contribution could be explained by reduced detection sensitivity and incomplete sequence coverage, as well as posttranslational modifications, which remain undetected [98]. In total, we identified five factors, of which factors 1 and 2 explain the majority of variance. Factor 1 showed a strong correlation with the genotype of the samples, separating DMD from WT SCs, the transcriptomic and proteomic signatures contributed almost equally. Factor 2 distinguished the samples based on their developmental state, with a higher contribution of the transcriptomic data to the observed variance.

Future studies should include a longitudinal analysis of SCs isolated at different ages of the model organism to provide a time-resolved analysis that could capture valuable insights into disease progression and identify crucial molecular events for precisely timed treatment interventions [99]. In addition to our results, single-cell sequencing approaches could help to identify SC subpopulations and reveal how dystrophin deficiency alters lineage trajectories to detect cell- and time-specific molecular markers that might not be uncovered in bulk analyses [69,70]. Given our observations in altered traction forces in DMD SCs, spatial investigations could further contemplate our data on in vitro force measurements by connecting the mechanical DMD SC phenotype to region-specific expression patterns of cell adhesion and force transmission-related genes [100].

5. Conclusions

To our knowledge, this is the first co-evaluation and integration of the transcriptomic and proteomic data of dystrophin-deficient SCs derived from a translational porcine model of DMD. We showed that the lack of dystrophin directly affects a plethora of aspects during myogenesis already coming into play at early developmental stages. Further, we demonstrated that dystrophin deficiency has functional consequences leading to higher forces exerted by the affected SCs at a single cell stage when they are still unexposed to contraction forces. Together, our findings support the hypothesis that intracellular deficits emerging from dystrophin deficiency account for SC dysfunctions in DMD. Lastly, our dataset represents a valuable basis for prospective investigations aiming to elucidate the functions and potential therapeutic targets amongst the identified genes and proteins.

Supplementary Materials: The following supporting information can be downloaded at https://www.mdpi.com/article/10.3390/cells14120892/s1, Method S1: Protocol for the isolation of porcine satellite cells from transgenic DMD and WT piglets; Table S1: Top differentially expressed genes between DMD and WT SCs in PROL state; Table S2: Top differentially expressed genes between DMD and WT SCs in DIFF state; Table S3: GO enrichment analysis using the BP database of differentially expressed genes between DMD and WT SCs in PROL state; Table S4: GO enrichment analysis using the BP database of differentially expressed genes between DMD and WT SCs in DIFF state; Table S5: Quantified proteins in DMD and WT SCs by LC-MS/MS; Table S6: Identified Proteins in DMD and WT SCs; Table S7: Differentially abundant proteins between DMD and WT in PROL state; Table S8: Differentially abundant proteins between DMD and WT in DIFF state; Figure S1: Negative controls for immunohistochemistry and immunofluorescence experiments and validation of myogenic

Cells 2025, 14, 892 23 of 28

nature of isolated SCs; Figure S2: Top 25 features for factor 1 and 2 in transcriptomic and proteomic dataset and their sample expression.

Author Contributions: Conceptualization, S.F., J.S., and K.M., with intellectual input from N.P., B.S., T.F., and E.W.; methodology, S.F., A.M., J.B.S., C.K., and M.S.; formal analysis and data curation, S.F., S.C., J.B.S., A.M., and J.J.; resources, N.P., B.S., T.F., E.W., C.K., and M.S.; writing—original draft preparation, S.F.; supervision, K.M., and J.S. All authors have read and agreed to the published version of the manuscript.

Funding: A.M. and B.S acknowledge funding from the European Research Council (ERC) under the European Union Horizon 2020 research and innovation program (G.A. 852585). The development and characterization of the porcine DMD model was funded by the Bayerische Forschungsstiftung (AZ 802-08; PDOC-90-15), by the Else Kröner-Fresenius-Stiftung (EKFS; 2015_180), by the ForTra gGmbH für Forschungstransfer der EKFS (2018_T20; 2022_EKSE.41), and—in part—by the Leducq Foundation (Network 23CVD01).

Institutional Review Board Statement: The animal study protocol was approved by the responsible welfare authority (Government of Upper Bavaria; permission ROB.55.2-2532.Vet_02-19-195) on 20 July 2020. All experiments were conducted in accordance with the German Animal Welfare Act and Directive 2010/63/EU on the protection of animals used for scientific purposes.

Informed Consent Statement: Not applicable.

Data Availability Statement: The TFM workflow and analysis script can be found at https://github.com/J-jianfei/TFM_workflow (accessed on 22 November 2024). The RNA-seq dataset supporting the conclusions of this article is available in the NCBI's Gene Expression Omnibus (GEO) [101] repository, GEO Series accession number GSE287756, https://www.ncbi.nlm.nih.gov/geo/query/acc.cgi?acc=GSE287756 (accessed on 22 November 2024). The mass spectrometry proteomic dataset generated during the current study is available in the ProteomeXchange Consortium via the PRIDE [102] partner repository, dataset identifier PXD059983.

Acknowledgments: The authors would like to thank all members of the laboratory who supported the project. We thank Lisa Pichl for her support during cell isolation and staining procedures. We thank Laura Steingruber and Patrizia Torelli for their help in cell isolation and cell culture work. We thank Sandra Baur for supporting general lab work related to cell culture, Western blot, and cell-staining protocols. We thank Kathrin Simon for her assistance during traction force measurements. We thank Eva Mayr for her expert RNA sequencing service. We also thank Miwoka Köster for technical assistance during proteomics measurements.

Conflicts of Interest: The authors declare no conflicts of interest.

Abbreviations

The following abbreviations are used in this manuscript:

ACT Actin

AKR1C1 Aldo-Keto Reductase Family 1 Member C1

ALDH Aldehyde dehydrogenase

BP Biological process

C3 Complement Component 3

CCK Cholecystokinin
CFH Complement Factor H

CNN1 Calponin 1 CORT Cortistatin

CYLC1 Cytoplasmic Linker Protein 1

DAB Diaminobenzidine tetrahydrochloride dihydrate

DES Desmin

DGC Dystrophin-associated glycoprotein complex

DIFF Differentiation

Cells 2025, 14, 892 24 of 28

DMD Duchenne muscular dystrophy

ECM Extracellular matrix

FMO1 Flavin-Containing Monooxygenase 1

GO Gene Ontology

GTP Guanosine Triphosphate

HECW2 HECT, C2 and WW domain-containing E3 ubiquitin protein ligase 2

HIF1α Hypoxia-Inducible Factor 1 Alpha

IgG Immunoglobulin G
INT Intercostalis muscle

ITG Integrin

LC-MS/MS Liquid chromatography tandem mass spectrometry

LF Latent factor

LGALS13 Lectin, Galactoside-Binding, Soluble, 13
MACF1 Microtubule Actin Crosslinking Factor 1
MACS Magnetically activated cell sorting

MARK2 Microtubule Affinity-Regulating Kinase 2

MOFA Multi-omics factor analysis MYF5 Myogenic regulatory factor 5 MYH Myosin Heavy Chain

MYL Myosin Heavy Chain

MYL Myosin Light Chain

MYLPF Myosin Light Chain Phosphatase, F subunit

MYOD1 Myoblast determination protein 1

MYOG Muscle-specific transcription factor myogenin

NCALD Neurocalcin Delta

PAQR6 Progestin and AdipoQ Receptor Family Member 6

PAX7 Paired box protein 7
PECT Pectoralis muscle
PPL Plakophilin 1
PROL Proliferation
SCs Satellite cells

SLC46A3 Solute Carrier Family 46 Member 3

TAGLN Transgelin

TFM Traction force microscopy

TGF-β Transforming Growth Factor Beta

TNN Troponin
TPM Tropomyosin 1
WT Wild type

References

- 1. Dumont, N.A.; Wang, Y.X.; von Maltzahn, J.; Pasut, A.; Bentzinger, C.F.; Brun, C.E.; Rudnicki, M.A. Dystrophin expression in muscle stem cells regulates their polarity and asymmetric division. *Nat. Med.* **2015**, *21*, 1455–1463. [CrossRef] [PubMed]
- 2. Yin, H.; Price, F.; Rudnicki, M.A. Satellite cells and the muscle stem cell niche. *Physiol. Rev.* 2013, 93, 23–67. [CrossRef]
- 3. Hildyard, J.C.W.; Roskrow, L.E.; Wells, D.J.; Piercy, R.J. Spatiotemporal analysis of dystrophin expression during muscle repair. *bioRxiv* **2024**. [CrossRef]
- 4. Kodippili, K.; Rudnicki, M.A. Satellite cell contribution to disease pathology in Duchenne muscular dystrophy. *Front. Physiol.* **2023**, *14*, 1180980. [CrossRef]
- 5. Gosselin, M.R.F.; Mournetas, V.; Borczyk, M.; Verma, S.; Occhipinti, A.; Rog, J.; Bozycki, L.; Korostynski, M.; Robson, S.C.; Angione, C.; et al. Loss of full-length dystrophin expression results in major cell-autonomous abnormalities in proliferating myoblasts. *eLife* 2022, 11, e75521. [CrossRef]
- 6. Kottlors, M.; Kirschner, J. Elevated satellite cell number in Duchenne muscular dystrophy. *Cell Tissue Res.* **2010**, 340, 541–548. [CrossRef] [PubMed]
- 7. Bankole, L.C.; Feasson, L.; Ponsot, E.; Kadi, F. Fibre type-specific satellite cell content in two models of muscle disease. *Histopathology* **2013**, *63*, 826–832. [CrossRef]

Cells 2025, 14, 892 25 of 28

8. Reimann, J.; Irintchev, A.; Wernig, A. Regenerative capacity and the number of satellite cells in soleus muscles of normal and mdx mice. *Neuromuscul. Disord.* **2000**, *10*, 276–282. [CrossRef] [PubMed]

- 9. Ribeiro, A.F., Jr.; Souza, L.S.; Almeida, C.F.; Ishiba, R.; Fernandes, S.A.; Guerrieri, D.A.; Santos, A.L.F.; Onofre-Oliveira, P.C.G.; Vainzof, M. Muscle satellite cells and impaired late stage regeneration in different murine models for muscular dystrophies. *Sci. Rep.* **2019**, *9*, 11842. [CrossRef]
- 10. Heslop, L.; Morgan, J.E.; Partridge, T.A. Evidence for a myogenic stem cell that is exhausted in dystrophic muscle. *J. Cell Sci.* **2000**, 113 *Pt* 12, 2299–2308. [CrossRef]
- 11. Luz, M.A.; Marques, M.J.; Santo Neto, H. Impaired regeneration of dystrophin-deficient muscle fibers is caused by exhaustion of myogenic cells. *Braz. J. Med. Biol. Res.* **2002**, *35*, 691–695. [CrossRef]
- 12. Dumont, N.A.; Rudnicki, M.A. Targeting muscle stem cell intrinsic defects to treat Duchenne muscular dystrophy. *npj Regen. Med.* **2016**, *1*, 16006. [CrossRef] [PubMed]
- 13. Sun, C.; Serra, C.; Lee, G.; Wagner, K.R. Stem cell-based therapies for Duchenne muscular dystrophy. *Exp. Neurol.* **2020**, 323, 113086. [CrossRef] [PubMed]
- 14. Mauro, A. Satellite cell of skeletal muscle fibers. J. Biophys. Biochem. Cytol. 1961, 9, 493–495. [CrossRef] [PubMed]
- 15. Relaix, F.; Bencze, M.; Borok, M.J.; Der Vartanian, A.; Gattazzo, F.; Mademtzoglou, D.; Perez-Diaz, S.; Prola, A.; Reyes-Fernandez, P.C.; Rotini, A.; et al. Perspectives on skeletal muscle stem cells. *Nat. Commun.* **2021**, *12*, 692. [CrossRef] [PubMed]
- 16. Buckingham, M.; Relaix, F. PAX3 and PAX7 as upstream regulators of myogenesis. *Semin. Cell Dev. Biol.* **2015**, 44, 115–125. [CrossRef] [PubMed]
- 17. Zammit, P.S. Function of the myogenic regulatory factors Myf5, MyoD, Myogenin and MRF4 in skeletal muscle, satellite cells and regenerative myogenesis. *Semin. Cell Dev. Biol.* **2017**, 72, 19–32. [CrossRef] [PubMed]
- 18. Ganassi, M.; Muntoni, F.; Zammit, P.S. Defining and identifying satellite cell-opathies within muscular dystrophies and myopathies. *Exp. Cell Res.* **2022**, 411, 112906. [CrossRef]
- 19. Ganassi, M.; Zammit, P.S. Involvement of muscle satellite cell dysfunction in neuromuscular disorders: Expanding the portfolio of satellite cell-opathies. *Eur. J. Transl. Myol.* **2022**, *32*, 10064. [CrossRef]
- 20. Emery, A.E.H. Population Frequencies of Inherited Neuromuscular Diseases—A World Survey. *Neuromuscul. Disord.* **1991**, 1, 19–29. [CrossRef]
- 21. Mendell, J.R.; Shilling, C.; Leslie, N.D.; Flanigan, K.M.; al-Dahhak, R.; Gastier-Foster, J.; Kneile, K.; Dunn, D.M.; Duval, B.; Aoyagi, A.; et al. Evidence-based path to newborn screening for Duchenne muscular dystrophy. *Ann. Neurol.* **2012**, *71*, 304–313. [CrossRef] [PubMed]
- 22. Happi Mbakam, C.; Tremblay, J.P. Gene therapy for Duchenne muscular dystrophy: An update on the latest clinical developments. *Expert Rev. Neurother.* **2023**, 23, 905–920. [CrossRef]
- 23. Gao, Q.Q.; McNally, E.M. The Dystrophin Complex: Structure, Function, and Implications for Therapy. *Compr. Physiol.* **2015**, 5, 1223–1239. [CrossRef]
- 24. Duan, D.; Goemans, N.; Takeda, S.; Mercuri, E.; Aartsma-Rus, A. Duchenne muscular dystrophy. *Nat. Rev. Dis. Primers* **2021**, *7*, 13. [CrossRef]
- 25. Fontelonga, T.M.; Jordan, B.; Nunes, A.M.; Barraza-Flores, P.; Bolden, N.; Wuebbles, R.D.; Griner, L.M.; Hu, X.; Ferrer, M.; Marugan, J.; et al. Sunitinib promotes myogenic regeneration and mitigates disease progression in the mdx mouse model of Duchenne muscular dystrophy. *Hum. Mol. Genet.* **2019**, *28*, 2120–2132. [CrossRef]
- 26. Passamano, L.; Taglia, A.; Palladino, A.; Viggiano, E.; D'Ambrosio, P.; Scutifero, M.; Rosaria Cecio, M.; Torre, V.; De Luca, F.; Picillo, E.; et al. Improvement of survival in Duchenne Muscular Dystrophy: Retrospective analysis of 835 patients. *Acta Myol.* **2012**, *31*, 121–125.
- 27. Wahlgren, L.; Kroksmark, A.K.; Tulinius, M.; Sofou, K. One in five patients with Duchenne muscular dystrophy dies from other causes than cardiac or respiratory failure. *Eur. J. Epidemiol.* **2022**, *37*, 147–156. [CrossRef] [PubMed]
- 28. McGreevy, J.W.; Hakim, C.H.; McIntosh, M.A.; Duan, D. Animal models of Duchenne muscular dystrophy: From basic mechanisms to gene therapy. *Dis. Models Mech.* **2015**, *8*, 195–213. [CrossRef] [PubMed]
- 29. Zaynitdinova, M.I.; Lavrov, A.V.; Smirnikhina, S.A. Animal models for researching approaches to therapy of Duchenne muscular dystrophy. *Transgenic Res.* **2021**, *30*, 709–725. [CrossRef]
- 30. Moretti, A.; Fonteyne, L.; Giesert, F.; Hoppmann, P.; Meier, A.B.; Bozoglu, T.; Baehr, A.; Schneider, C.M.; Sinnecker, D.; Klett, K.; et al. Somatic gene editing ameliorates skeletal and cardiac muscle failure in pig and human models of Duchenne muscular dystrophy. *Nat. Med.* **2020**, *26*, 207–214. [CrossRef]
- 31. Stirm, M.; Fonteyne, L.M.; Shashikadze, B.; Lindner, M.; Chirivi, M.; Lange, A.; Kaufhold, C.; Mayer, C.; Medugorac, I.; Kessler, B.; et al. A scalable, clinically severe pig model for Duchenne muscular dystrophy. *Dis. Models Mech.* **2021**, *14*, dmm049285. [CrossRef] [PubMed]
- 32. Stirm, M.; Klymiuk, N.; Nagashima, H.; Kupatt, C.; Wolf, E. Pig models for translational Duchenne muscular dystrophy research. *Trends Mol. Med.* **2024**, *30*, 950–964. [CrossRef] [PubMed]

Cells 2025, 14, 892 26 of 28

33. Klymiuk, N.; Blutke, A.; Graf, A.; Krause, S.; Burkhardt, K.; Wuensch, A.; Krebs, S.; Kessler, B.; Zakhartchenko, V.; Kurome, M.; et al. Dystrophin-deficient pigs provide new insights into the hierarchy of physiological derangements of dystrophic muscle. *Hum. Mol. Genet.* **2013**, 22, 4368–4382. [CrossRef]

- 34. Ding, S.; Wang, F.; Liu, Y.; Li, S.; Zhou, G.; Hu, P. Characterization and isolation of highly purified porcine satellite cells. *Cell Death Discov.* **2017**, *3*, 17003. [CrossRef]
- 35. Holenstein, C.N.; Silvan, U.; Snedeker, J.G. High-resolution traction force microscopy on small focal adhesions—Improved accuracy through optimal marker distribution and optical flow tracking. *Sci. Rep.* **2017**, *7*, 41633. [CrossRef] [PubMed]
- 36. Huang, Y.; Schell, C.; Huber, T.B.; Şimşek, A.N.; Hersch, N.; Merkel, R.; Gompper, G.; Sabass, B. Traction force microscopy with optimized regularization and automated Bayesian parameter selection for comparing cells. *Sci. Rep.* **2019**, *9*, 539. [CrossRef]
- 37. Picelli, S.; Bjorklund, A.K.; Faridani, O.R.; Sagasser, S.; Winberg, G.; Sandberg, R. Smart-seq2 for sensitive full-length transcriptome profiling in single cells. *Nat. Methods* **2013**, *10*, 1096–1098. [CrossRef]
- 38. Picelli, S.; Faridani, O.R.; Bjorklund, A.K.; Winberg, G.; Sagasser, S.; Sandberg, R. Full-length RNA-seq from single cells using Smart-seq2. *Nat. Protoc.* **2014**, *9*, 171–181. [CrossRef]
- 39. Bagnoli, J.W.; Ziegenhain, C.; Janjic, A.; Wange, L.E.; Vieth, B.; Parekh, S.; Geuder, J.; Hellmann, I.; Enard, W. Sensitive and powerful single-cell RNA sequencing using mcSCRB-seq. *Nat. Commun.* **2018**, *9*, 2937. [CrossRef]
- 40. Andrews, S. A Quality Control Tool for High Throughput Sequence Data. 2010. Available online: http://www.bioinformatics.babraham.ac.uk/projects/fastqc/ (accessed on 16 October 2023).
- 41. Ewels, P.; Magnusson, M.; Lundin, S.; Käller, M. MultiQC: Summarize analysis results for multiple tools and samples in a single report. *Bioinformatics* **2016**, *32*, 3047–3048. [CrossRef]
- 42. Smith, T.; Heger, A.; Sudbery, I. UMI-tools: Modeling sequencing errors in Unique Molecular Identifiers to improve quantification accuracy. *Genome Res.* **2017**, 27, 491–499. [CrossRef] [PubMed]
- 43. Dobin, A.; Davis, C.A.; Schlesinger, F.; Drenkow, J.; Zaleski, C.; Jha, S.; Batut, P.; Chaisson, M.; Gingeras, T.R. STAR: Ultrafast universal RNA-seq aligner. *Bioinformatics* **2013**, *29*, 15–21. [CrossRef] [PubMed]
- 44. Robinson, M.D.; McCarthy, D.J.; Smyth, G.K. edgeR: A Bioconductor package for differential expression analysis of digital gene expression data. *Bioinformatics* **2010**, *26*, 139–140. [CrossRef] [PubMed]
- 45. Korotkevich, G.; Sukhov, V.; Budin, N.; Shpak, B.; Artyomov, M.N.; Sergushichev, A. Fast gene set enrichment analysis. *bioRxiv* **2021**. [CrossRef]
- 46. Cox, J.; Mann, M. MaxQuant enables high peptide identification rates, individualized p.p.b.-range mass accuracies and proteomewide protein quantification. *Nat. Biotechnol.* **2008**, *26*, 1367–1372. [CrossRef]
- 47. Signorelli, M.; Tsonaka, R.; Aartsma-Rus, A.; Spitali, P. Multiomic characterization of disease progression in mice lacking dystrophin. *PLoS ONE* **2023**, *18*, e0283869. [CrossRef] [PubMed]
- 48. Tyanova, S.; Temu, T.; Sinitcyn, P.; Carlson, A.; Hein, M.Y.; Geiger, T.; Mann, M.; Cox, J. The Perseus computational platform for comprehensive analysis of (prote)omics data. *Nat. Methods* **2016**, *13*, 731–740. [CrossRef]
- 49. Ropka-Molik, K.; Eckert, R.; Piorkowska, K. The expression pattern of myogenic regulatory factors MyoD, Myf6 and Pax7 in postnatal porcine skeletal muscles. *Gene Expr. Patterns* **2011**, *11*, 79–83. [CrossRef]
- 50. Zammit, P.S.; Relaix, F.; Nagata, Y.; Ruiz, A.P.; Collins, C.A.; Partridge, T.A.; Beauchamp, J.R. Pax7 and myogenic progression in skeletal muscle satellite cells. *J. Cell Sci.* **2006**, *119*, 1824–1832. [CrossRef]
- 51. Jiang, C.; Wen, Y.; Kuroda, K.; Hannon, K.; Rudnicki, M.A.; Kuang, S. Notch signaling deficiency underlies age-dependent depletion of satellite cells in muscular dystrophy. *Dis. Models Mech.* **2014**, *7*, 997–1004. [CrossRef]
- 52. Yang, J.; Liu, H.; Wang, K.; Li, L.; Yuan, H.; Liu, X.; Liu, Y.; Guan, W. Isolation, culture and biological characteristics of multipotent porcine skeletal muscle satellite cells. *Cell Tissue Bank.* **2017**, *18*, 513–525. [CrossRef] [PubMed]
- 53. Paulin, D.; Li, Z. Desmin: A major intermediate filament protein essential for the structural integrity and function of muscle. *Exp. Cell Res.* **2004**, *301*, 1–7. [CrossRef] [PubMed]
- 54. Asfour, H.A.; Allouh, M.Z.; Said, R.S. Myogenic regulatory factors: The orchestrators of myogenesis after 30 years of discovery. *Exp. Biol. Med.* **2018**, 243, 118–128. [CrossRef] [PubMed]
- 55. Shirakawa, T.; Toyono, T.; Inoue, A.; Matsubara, T.; Kawamoto, T.; Kokabu, S. Factors Regulating or Regulated by Myogenic Regulatory Factors in Skeletal Muscle Stem Cells. *Cells* **2022**, *11*, 1493. [CrossRef]
- 56. Bruyere, C.; Versaevel, M.; Mohammed, D.; Alaimo, L.; Luciano, M.; Vercruysse, E.; Gabriele, S. Actomyosin contractility scales with myoblast elongation and enhances differentiation through YAP nuclear export. *Sci. Rep.* **2019**, *9*, 15565. [CrossRef]
- 57. Chang, N.C.; Chevalier, F.P.; Rudnicki, M.A. Satellite Cells in Muscular Dystrophy—Lost in Polarity. *Trends Mol. Med.* **2016**, 22, 479–496. [CrossRef] [PubMed]
- 58. Zettler, S.; Renner, S.; Kemter, E.; Hinrichs, A.; Klymiuk, N.; Backman, M.; Riedel, E.O.; Mueller, C.; Streckel, E.; Braun-Reichhart, C.; et al. A decade of experience with genetically tailored pig models for diabetes and metabolic research. *Anim. Reprod.* 2020, 17, e20200064. [CrossRef]

Cells 2025, 14, 892 27 of 28

59. Stirm, M.; Fonteyne, L.M.; Shashikadze, B.; Stockl, J.B.; Kurome, M.; Kessler, B.; Zakhartchenko, V.; Kemter, E.; Blum, H.; Arnold, G.J.; et al. Pig models for Duchenne muscular dystrophy—From disease mechanisms to validation of new diagnostic and therapeutic concepts. *Neuromuscul. Disord.* 2022, 32, 543–556. [CrossRef]

- 60. Lo Mauro, A.; Aliverti, A. Physiology of respiratory disturbances in muscular dystrophies. Breathe 2016, 12, 318–327. [CrossRef]
- 61. Baig, M.A.; Bordoni, B. Anatomy, Shoulder and Upper Limb, Pectoral Muscles. In *StatPearls*; StatPearls Publishing LLC: Treasure Island, FL, USA, 2024.
- 62. Burmeister, D.M.; Supp, D.M.; Clark, R.A.; Tredget, E.E.; Powell, H.M.; Enkhbaatar, P.; Bohannon, J.K.; Cancio, L.C.; Hill, D.M.; Nygaard, R.M. Advantages and Disadvantages of Using Small and Large Animals in Burn Research: Proceedings of the 2021 Research Special Interest Group. *J. Burn Care Res.* 2022, 43, 1032–1041. [CrossRef]
- 63. Hou, N.; Du, X.; Wu, S. Advances in pig models of human diseases. Anim. Models Exp. Med. 2022, 5, 141–152. [CrossRef]
- 64. Agley, C.C.; Rowlerson, A.M.; Velloso, C.P.; Lazarus, N.L.; Harridge, S.D. Isolation and quantitative immunocytochemical characterization of primary myogenic cells and fibroblasts from human skeletal muscle. *J. Vis. Exp.* **2015**, *95*, e52049. [CrossRef]
- 65. Syverud, B.C.; Lee, J.D.; VanDusen, K.W.; Larkin, L.M. Isolation and Purification of Satellite Cells for Skeletal Muscle Tissue Engineering. *J. Regen. Med.* **2014**, *3*, 117. [CrossRef] [PubMed]
- 66. Dan-Jumbo, S.O.; Riley, S.E.; Cortes-Araya, Y.; Ho, W.; Lee, S.; Thrower, T.; Esteves, C.L.; Donadeu, F.X. Derivation and long-term maintenance of porcine skeletal muscle progenitor cells. *Sci. Rep.* **2024**, *14*, 9370. [CrossRef]
- 67. Vacanti, V.; Kong, E.; Suzuki, G.; Sato, K.; Canty, J.M.; Lee, T. Phenotypic changes of adult porcine mesenchymal stem cells induced by prolonged passaging in culture. *J. Cell. Physiol.* **2005**, 205, 194–201. [CrossRef] [PubMed]
- 68. Chen, J.; Xu, J.; Gou, L.; Zhu, Y.; Zhong, W.; Guo, H.; Du, Y. Integrating transcriptomic and proteomic data for a comprehensive molecular perspective on the association between sarcopenia and osteoporosis. *Arch. Gerontol. Geriatr.* **2024**, 125, 105486. [CrossRef] [PubMed]
- 69. Ahmad, R.; Budnik, B. A review of the current state of single-cell proteomics and future perspective. *Anal. Bioanal. Chem.* **2023**, 415, 6889–6899. [CrossRef]
- 70. Cha, J.; Lee, I. Single-cell network biology for resolving cellular heterogeneity in human diseases. *Exp. Mol. Med.* **2020**, 52, 1798–1808. [CrossRef]
- 71. Blau, H.M.; Webster, C.; Pavlath, G.K. Defective myoblasts identified in Duchenne muscular dystrophy. *Proc. Natl. Acad. Sci. USA* 1983, 80, 4856–4860. [CrossRef]
- 72. Hurko, O.; McKee, L.; Zuurveld, J.; Swick, H.M. Comparison of Duchenne and normal myoblasts from a heterozygote. *Neurology* **1987**, 37, 675. [CrossRef]
- 73. Mournetas, V.; Massouridès, E.; Dupont, J.B.; Kornobis, E.; Polvèche, H.; Jarrige, M.; Dorval, A.R.L.; Gosselin, M.R.F.; Manousopoulou, A.; Garbis, S.D.; et al. Myogenesis modelled by human pluripotent stem cells: A multi-omic study of Duchenne myopathy early onset. *J. Cachexia Sarcopenia Muscle* 2021, 12, 209–232. [CrossRef] [PubMed]
- 74. Górecki, D.C. Dystrophin: The dead calm of a dogma. Rare Dis. 2016, 4, e1153777. [CrossRef] [PubMed]
- 75. Seale, P.; Sabourin, L.A.; Girgis-Gabardo, A.; Mansouri, A.; Gruss, P.; Rudnicki, M.A. Pax7 is required for the specification of myogenic satellite cells. *Cell* **2000**, *102*, 777–786. [CrossRef]
- 76. Filippelli, R.L.; Chang, N.C. Empowering Muscle Stem Cells for the Treatment of Duchenne Muscular Dystrophy. *Cells Tissues Organs* **2022**, 211, 641–654. [CrossRef]
- 77. Wang, Y.X.; Feige, P.; Brun, C.E.; Hekmatnejad, B.; Dumont, N.A.; Renaud, J.M.; Faulkes, S.; Guindon, D.E.; Rudnicki, M.A. EGFR-Aurka Signaling Rescues Polarity and Regeneration Defects in Dystrophin-Deficient Muscle Stem Cells by Increasing Asymmetric Divisions. *Cell Stem Cell* 2019, 24, 419–432.e416. [CrossRef]
- 78. Ervasti, J.M. Dystrophin, its interactions with other proteins, and implications for muscular dystrophy. *Biochim. Biophys. Acta* **2007**, 1772, 108–117. [CrossRef] [PubMed]
- 79. Hofemeier, A.D.; Muenker, T.M.; Herkenrath, F.; Ristau, M.; Brandt, M.; Shahriyari, M.; Tiburcy, M.; Zimmermann, W.H.; Lenz, C.; Mamchaoui, K.; et al. Dystrophin is a mechanical tension modulator. *bioRxiv* **2022**. [CrossRef]
- 80. Pang, K.T.; Loo, L.S.W.; Chia, S.; Ong, F.Y.T.; Yu, H.; Walsh, I. Insight into muscle stem cell regeneration and mechanobiology. Stem Cell Res. Ther. 2023, 14, 129. [CrossRef]
- 81. Loreti, M.; Sacco, A. The jam session between muscle stem cells and the extracellular matrix in the tissue microenvironment. *npj Regen. Med.* **2022**, *7*, 16. [CrossRef]
- 82. Lu, P.; Takai, K.; Weaver, V.M.; Werb, Z. Extracellular matrix degradation and remodeling in development and disease. *Cold Spring Harb. Perspect. Biol.* **2011**, *3*, a005058. [CrossRef]
- 83. Daley, W.P.; Peters, S.B.; Larsen, M. Extracellular matrix dynamics in development and regenerative medicine. *J. Cell Sci.* **2008**, 121, 255–264. [CrossRef] [PubMed]
- 84. Biressi, S.; Miyabara, E.H.; Gopinath, S.D.; Carlig, P.M.; Rando, T.A. A Wnt-TGFbeta2 axis induces a fibrogenic program in muscle stem cells from dystrophic mice. *Sci. Transl. Med.* **2014**, *6*, 267ra176. [CrossRef]

Cells 2025, 14, 892 28 of 28

85. Giovarelli, M.; Arnaboldi, F.; Zecchini, S.; Cornaghi, L.B.; Nava, A.; Sommariva, M.; Clementi, E.G.I.; Gagliano, N. Characterisation of Progressive Skeletal Muscle Fibrosis in the Mdx Mouse Model of Duchenne Muscular Dystrophy: An In Vivo and In Vitro Study. *Int. J. Mol. Sci.* 2022, 23, 8735. [CrossRef]

- 86. Ramirez, M.P.; Anderson, M.J.M.; Kelly, M.D.; Sundby, L.J.; Hagerty, A.R.; Wenthe, S.J.; Odde, D.J.; Ervasti, J.M.; Gordon, W.R. Dystrophin missense mutations alter focal adhesion tension and mechanotransduction. *Proc. Natl. Acad. Sci. USA* **2022**, 119, e2205536119. [CrossRef]
- 87. Engler, A.J.; Griffin, M.A.; Sen, S.; Bönnemann, C.G.; Sweeney, H.L.; Discher, D.E. Myotubes differentiate optimally on substrates with tissue-like stiffness: Pathological implications for soft or stiff microenvironments. *J. Cell Biol.* **2004**, *166*, 877–887. [CrossRef]
- 88. Yamamoto, M.; Legendre, N.P.; Biswas, A.A.; Lawton, A.; Yamamoto, S.; Tajbakhsh, S.; Kardon, G.; Goldhamer, D.J. Loss of MyoD and Myf5 in Skeletal Muscle Stem Cells Results in Altered Myogenic Programming and Failed Regeneration. *Stem Cell Rep.* **2018**, 10, 956–969. [CrossRef] [PubMed]
- 89. Zammit, P.S.; Carvajal, J.J.; Golding, J.P.; Morgan, J.E.; Summerbell, D.; Zolnerciks, J.; Partridge, T.A.; Rigby, P.W.; Beauchamp, J.R. Myf5 expression in satellite cells and spindles in adult muscle is controlled by separate genetic elements. *Dev. Biol.* **2004**, 273, 454–465. [CrossRef]
- 90. Abdul-Hussein, S.; van der Ven, P.F.M.; Tajsharghi, H. Expression profiles of muscle disease-associated genes and their isoforms during differentiation of cultured human skeletal muscle cells. *BMC Musculoskelet. Disord.* **2012**, *13*, 262. [CrossRef] [PubMed]
- 91. Nguyen, T.-H.; Paprzycki, L.; Legrand, A.; Declèves, A.-E.; Heher, P.; Limpens, M.; Belayew, A.; Banerji, C.R.S.; Zammit, P.S.; Tassin, A. Hypoxia enhances human myoblast differentiation: Involvement of HIF1α and impact of DUX4, the FSHD causal gene. *Skelet. Muscle* **2023**, *13*, 21. [CrossRef]
- 92. Lundby, C.; Calbet, J.A.; Robach, P. The response of human skeletal muscle tissue to hypoxia. *Cell. Mol. Life Sci.* **2009**, *66*, 3615–3623. [CrossRef]
- 93. Sun, Z.; Guo, S.S.; Fassler, R. Integrin-mediated mechanotransduction. J. Cell Biol. 2016, 215, 445–456. [CrossRef] [PubMed]
- 94. Anastasi, G.; Amato, A.; Tarone, G.; Vita, G.; Monici, M.C.; Magaudda, L.; Brancaccio, M.; Sidoti, A.; Trimarchi, F.; Favaloro, A.; et al. Distribution and localization of vinculin-talin-integrin system and dystrophin-glycoprotein complex in human skeletal muscle. Immunohistochemical study using confocal laser scanning microscopy. *Cells Tissues Organs* **2003**, *175*, 151–164. [CrossRef]
- 95. Wilson, D.G.S.; Tinker, A.; Iskratsch, T. The role of the dystrophin glycoprotein complex in muscle cell mechanotransduction. *Commun. Biol.* **2022**, *5*, 1022. [CrossRef]
- 96. Steingruber, L.; Krabichler, F.; Franzmeier, S.; Wu, W.; Schlegel, J.; Koch, M. ALDH1A1 and ALDH1A3 paralogues of aldehyde dehydrogenase 1 control myogenic differentiation of skeletal muscle satellite cells by retinoic acid-dependent and -independent mechanisms. *Cell Tissue Res.* **2023**, *394*, 515–528. [CrossRef]
- 97. Argelaguet, R.; Velten, B.; Arnol, D.; Dietrich, S.; Zenz, T.; Marioni, J.C.; Buettner, F.; Huber, W.; Stegle, O. Multi-Omics Factor Analysis-a framework for unsupervised integration of multi-omics data sets. *Mol. Syst. Biol.* 2018, 14, e8124. [CrossRef] [PubMed]
- 98. Ladakis, D.C.; Pedrini, E.; Reyes-Mantilla, M.I.; Sanjayan, M.; Smith, M.D.; Fitzgerald, K.C.; Pardo, C.A.; Reich, D.S.; Absinta, M.; Bhargava, P. Metabolomics of Multiple Sclerosis Lesions Demonstrates Lipid Changes Linked to Alterations in Transcriptomics-Based Cellular Profiles. *Neurol. Neuroimmunol. Neuroinflamm.* 2024, 11, e200219. [CrossRef] [PubMed]
- 99. Moore, J.; Wu, T.; Dhindsa, J.; El Fadel, O.; Le, A.; Perez, A.; Amoh, B.; Tarkunde, A.; Zhu, K.F.; Avalos, M.; et al. Longitudinal multi-omics in alpha-synuclein Drosophila model discriminates disease- from age-associated pathologies in Parkinson's disease. *npj Park. Dis.* **2025**, *11*, 46. [CrossRef]
- 100. Bingham, G.C.; Lee, F.; Naba, A.; Barker, T.H. Spatial-omics: Novel approaches to probe cell heterogeneity and extracellular matrix biology. *Matrix Biol.* **2020**, *91*–*92*, 152–166. [CrossRef]
- 101. Edgar, R.; Domrachev, M.; Lash, A.E. Gene Expression Omnibus: NCBI gene expression and hybridization array data repository. *Nucleic Acids Res.* **2002**, 30, 207–210. [CrossRef]
- 102. Perez-Riverol, Y.; Bandla, C.; Kundu, D.J.; Kamatchinathan, S.; Bai, J.; Hewapathirana, S.; John, N.S.; Prakash, A.; Walzer, M.; Wang, S.; et al. The PRIDE database at 20 years: 2025 update. *Nucleic Acids Res.* **2025**, *53*, D543–D553. [CrossRef]

Disclaimer/Publisher's Note: The statements, opinions and data contained in all publications are solely those of the individual author(s) and contributor(s) and not of MDPI and/or the editor(s). MDPI and/or the editor(s) disclaim responsibility for any injury to people or property resulting from any ideas, methods, instructions or products referred to in the content.